การปรับปรุงเสถียรภาพทางความร้อนและการลดอันตรกิริยาของลิเทียมโบโรไฮไดรด์และพอลิเมอร์หลังการเติมโซเดียมอะลูมิเนียมไฮไดรด์ในการบรรจุระดับนาโนของลิเทียมโบโรไฮไดรด์ในพอลิเมทิลเมทาคริเลต-โค-บิวทิลเมทาคริเลต

นางสาวนันท์ธิดา วิเศษ

IMPROVEMENT OF THERMAL STABILITY
AND REDUCTION OF LiBH₄/POLYMER INTERACTION
AFTER NaAlH₄ DOPING IN NANOCONFINED LiBH₄–
POLY (METHYL METHACRYLATE)-co-BUTYL
METHACRYLATE

Nuntida Wiset

A Thesis Submitted in Partial Fulfillment of the Requirements for the

Degree of Master of Science in Chemistry

Suranaree University of Technology

Academic Year 2014

IMPROVEMENT OF THERMAL STABILITY

AND REDUCTION OF LiBH$_4$/POLYMER INTERACTION AFTER

NaAlH$_4$ DOPING IN NANOCONFINED LiBH$_4$– POLY (METHYL

METHACRYLATE)-co-BUTYL METHACRYLATE

Suranaree University of Technology has approved this thesis submitted in partial fulfillment of the requirements for a Master's Degree.

Thesis Examining Committee

_____

(Asst. Prof. Dr. Sanchai Prayoonpokarach)

Chairperson

_____

(Asst. Prof. Dr. Rapee Gosalawit-Utke)

Member (Thesis Advisor)

_____

(Asst. Prof. Dr. Kunwadee Rangsriwatananon)

Member

_____

(Dr. Theeranun Siritanon)

Member

_____   _____

(Prof. Dr. Sukit Limpijumnong)   (Assoc. Prof. Dr. Prapun Manyum)

Vice Rector for Academic Affairs   Dean of Institute of Science

and Innovation

นันท์ธิดา วิเศษ : การปรับปรุงเสถียรภาพทางความร้อนและการลดอันตรกิริยาของลิเทียม
โบโรไฮไดรด์และพอลิเมอร์หลังการเติมโซเดียมอะลูมิเนียมไฮไดรด์ในการบรรจุระดับนา
โนของลิเทียมโบโรไฮไดรด์ในพอลิเมทิลเมทาคริเลต-โค-บิวทิลเมทาคริเลต
(IMPROVEMENT OF THERMAL STABILITY AND REDUCTION OF
LiBH$_4$/POLYMER INTERACTION AFTER NaAlH$_4$ DOPING IN NANOCONFINED
LiBH$_4$–POLY (METHYL METHACRYLATE)-co-BUTYL METHACRYLATE)
อาจารย์ที่ปรึกษา : ผู้ช่วยศาสตราจารย์ ดร.ระพี โกศัลวิตร-อูทเคอ, 68 หน้า.

โซเดียมอะลูมิเนียมไฮไดรด์ที่ถูกเติมลงไปในลิเทียมโบโรไฮไดรด์บรรจุในระดับนาโนใน
พอลิเมทิลเมทาคริเลต-โค-บิวทิลเมทาคริเลต ถูกคาดหวังให้เป็นระบบกักเก็บไฮโดรเจนที่ผันกลับ
ได้ การปรับปรุงเสถียรภาพทางความร้อนและการลดอันตรกิริยาของลิเทียมโบโรไฮไดรด์และพอลิ
เมอร์ของตัวอย่างก็ถูกคาดหวังหลังการเติมโซเดียมอะลูมิเนียมไฮไดรด์ การลดอันตรกิริยาของ
ลิเทียมโบโรไฮไดรด์และพอลิเมอร์ของตัวอย่างจะถูกวิเคราะห์เชิงปริมาณโดยใช้เทคนิค FTIR ซึ่ง
จะศึกษาโดยการหาอัตราส่วนของพื้นที่ใต้พีคของ (ν(B–H)/ν(C=O)) ซึ่งจะสอดคล้องกับปริมาณ
ของโบโรไฮไดรด์ [BH$_4$]$^-$ การมีอัตราส่วนของ (ν(B–H)/ν(C=O)) มากจะส่งผลให้มีปริมาณของ
โบโรไฮไดรด์สำหรับปลดปล่อยไฮโดรเจนมากด้วย และอันตรกิริยาของลิเทียมโบโรไฮไดรด์และ
พอลิเมอร์ก็จะลดลงด้วย จากการเติมโซเดียมอะลูมิเนียมไฮไดรด์ อันตรกิริยาของลิเทียมโบโรไฮ-
ไดรด์และพอลิเมอร์ถูกทำให้ลดลงซึ่งจะสอดคล้องกับผลของ B 1s XPS ปริมาณของอันตรกิริยา
ของโบรอนและพอลิเมอร์ที่ได้จากตัวอย่างที่มีการเติมโซเดียมอะลูมิเนียมไฮไดรด์น้อยกว่าเมื่อเทียบ
กับตัวอย่างที่ไม่ได้เติมโซเดียมอะลูมิเนียมไฮไดรด์ นอกจากนี้ผลของ solid state MAS NMR และ
XRD ก็ยืนยันอีกด้วยว่าอันตรกิริยาของลิเทียมโบโรไฮไดรด์และพอลิเมอร์ถูกทำให้ลดลง เนื่องจาก
อะลูมิเนียมไฮไดรด์ [AlH$_4$]$^-$ของโซเดียมอะลูมิเนียมไฮไดรด์มาแข่งขันเกิดอันตรกิริยากับหมู่
เมทอกซีหรือหมู่บิวทอกซีของพอลิเมอร์ จึงส่งผลให้ปริมาณไฮโดรเจนที่ถูกปลดปล่อยออกมาจาก
การเกิดปฏิกิริยาการปล่อยไฮโดรเจนในรอบแรกและรอบที่สองมีปริมาณเพิ่มขึ้น นอกจากนี้พบว่ามี
การเกิดอันตรกิริยาระหว่างหมู่เมทอกซีของพอลิเมอร์กับโลหะไฮไดรด์ (ลิเทียมโบโรไฮไดรด์และ
โซเดียมอะลูมิเนียมไฮไดรด์) และการเกิดอันตรกิริยาระหว่างหมู่คาร์บอนิลของพอลิเมอร์กับโลหะ
ไอออน (Li$^+$ และ Na$^+$) ซึ่งจะช่วยเพิ่มความเสถียรภาพทางความร้อนของพอลิเมอร์ ดังนั้นปริมาณ
การปลดปล่อยแก๊สทั้งหมดที่เกิดจากการสลายตัวของพอลิเมอร์ของตัวอย่างที่มีการเติมโซเดียม-
อะลูมิเนียมไฮไดรด์จะปล่อยน้อยกว่าตัวอย่างที่ไม่ได้เติมโซเดียมอะลูมิเนียมไฮไดรด์

สาขาวิชาเคมี   ลายมือชื่อนักศึกษา_____
ปีการศึกษา 2557   ลายมือชื่ออาจารย์ที่ปรึกษา_____

NUNTIDA WISET : IMPROVEMENT OF THERMAL STABILITY AND
REDUCTION OF LiBH$_4$/POLYMER INTERACTION AFTER NaAlH$_4$
DOPING IN NANOCONFINED LiBH$_4$–POLY (METHYL
METHACRYLATE)-co-BUTYL METHACRYLATE. THESIS ADVISOR :
ASST. PROF. RAPEE GOSALAWIT-UTKE, Ph.D. 68 PP.

THERMAL STABILITY / POLYMER HOSTS / NANOCONFINEMENT /
HYDRIDE-POLYMER INTERACTION / LITHIUMBOROHYDRIDE /
SODIUMALUMINIUMHYDRIDE

NaAlH$_4$ doped into nanoconfined LiBH$_4$ in poly (methyl methacrylate)-co-
butyl methacrylate (PcB), denoted as nano LiBH$_4$−NaAlH$_4$−PcB, is proposed for
reversible hydrogen storage. The reduction of LiBH$_4$/PcB interaction (B---OCH$_3$) and
improvement of thermal stability of PcB are expected to obtain by adding small
amount of NaAlH$_4$. The LiBH$_4$/PcB interaction of the nanoconfined samples is
analyzed quantitatively by using FTIR technique, where the ν(B–H)/ν(C=O) ratio
directly related to the amount of [BH$_4$]$^-$ is determined. The more the (ν(B–H)/ν(C=O))
ratio, the higher the free [BH$_4$]$^-$ content and the lower the LiBH$_4$/PcB interaction. The
(ν(B–H)/ν(C=O)) ratio of the nano LiBH$_4$–PcB and nano LiBH$_4$–NaAlH$_4$–PcB are 0.6
and 2.8, respectively. This refers to the reduction of LiBH$_4$/PcB interaction due to
addition of NaAlH$_4$. This is in agreement with B 1s XPS results, the relative amount
of B$_x$O$_y$ (from LiBH$_4$/PcB interaction) with respect to LiBH$_4$ of nano LiBH$_4$–
NaAlH$_4$–PcB is lower than that of nano LiBH$_4$–PcB. In addition, the solid state MAS
NMR and XRD results of nano LiBH$_4$–NaAlH$_4$–PcB confirms that the LiBH$_4$/PcB

interaction is decreased due to the competitive reaction of $[AlH_4]^-$ (of $NaAlH_4$) with $-OCH_3$ and/or $-OC_4H_9$ (of PcB). These results increase of H_2 content dehydrogenated during cycling. Moreover, the interaction between alkoxy groups ($-OCH_3$ and/or $-OC_4H_9$) of PcB and metal hydrides ($LiBH_4$ and $NaAlH_4$) as well as that between carbonyl group (from PcB) and metal ions (Li^+ and Na^+) result in the improvement of thermal stability of PcB.

School of Chemistry	Student's Signature_____
Academic Year 2014	Advisor's Signature_____

ACKNOWLEDGEMENTS

CONTENTS

CONTENTS (Continued)

CONTENTS (Continued)

LIST OF TABLES

LIST OF FIGURES

LIST OF FIGURES (Continued)

LIST OF ABBREVIATIONS

ºC	=	degree celsius
µs	=	micro second
2θ	=	two theta
cm^{-1}	=	wavenumber
eV	=	electron volt
g	=	gram
h	=	hour
K	=	Kelvin
$kgH_2\,m^{-3}$	=	kilograms of hydrogen per cubic meter
kHz	=	kilohertz
L	=	liter
M	=	molar
mA	=	mill ampare
mg	=	milligram
min	=	minute
$MJ\,kg^{-1}$	=	megajoules per kilogram
mL	=	milliliter
MPa	=	megapascal
mV	=	millivolt
MW	=	molecular weight

LIST OF ABBREVIATIONS (Continued)

ppm	=	part per million
s	=	second
w/v	=	weight by volume

CHAPTER I

INTRODUCTION

1.1 Renewable energy technology

Energy sources

Energy can be obtained from different sources, such as chemical (fossil fuels), solar (photovoltaic cell), nuclear (uranium) and thermo mechanical (wind, water and hot water) energy. Each kind of energy has its own problems. For example, the use of fossil fuels leads to the production of the greenhouse gas (CO_2). This causes global warming and climate change (Environmental and Energy Study Institute, www, 2014). For the nuclear energy, the problem is nuclear wastes (Problems and Dangers of Nuclear Energy, www, 2014), while solar and wind energy require the use of large areas (Michael, 2014).

Currently, fossil fuel and nuclear sources are the main energy suppliers for the world. The high consumption of fossil fuel is expected to enhance the greenhouse gas (CO_2) in the atmosphere and to deplete fossil fuel supplies in the coming decades. The continuous emission of CO_2, which leads to world warming, is a serious problem for the global environment. Also, in the coming century, the world population is supposed to be increased together with a rapid growth of the economies. Thus, this will result in a higher demand of the energy consumption of the world. In order to meet the growth of energy requirement, while producing less CO_2, the current energy

of fossil fuels has to be replaced by new environmental friendly sources, such as solar, geothermal, wind, and hydrogen energy (Energy Resources, www, 2014).

1.2   Hydrogen energy

Hydrogen is one of the most promising energy carriers, which can potentially replace fossil fuels as sources of clean energy due to high energy density of 142 MJ kg^{-1} (Jain *et al*., 2010), light weight, great variety of potential sources (water, biomass, and organic matter), and low environmental impact (water and heat are by-product). Hydrogen energy is mainly used in fuel cells for various applications, such as electric power, transportation, industry, and public welfare. Good example is hydrogen car (Figure 1.1), planned to be worldwide sold by Honda and Toyota in 2015.
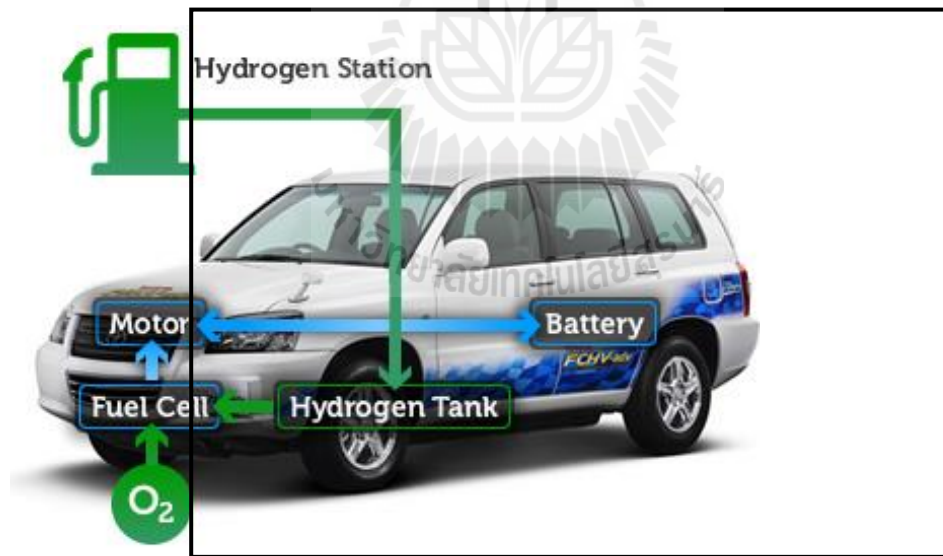
Figure 1.1 Components of fuel cell car (http://www.engineering.com/DesignerEdge/ DesignerEdgeArticles/ArticleID/5974/Hydrogen-Powered-Cars-Coming-to-ahighway -near-you.aspx).

Fuel cell car includes four major components of:

1. fuel cell stack: the fuel cell is an electrochemical device that produces electricity using hydrogen and oxygen. To obtain enough electricity to power a vehicle, individual fuel cells are combined in series to make a fuel cell stack,

2. hydrogen tank: instead of a gasoline or diesel tank, a fuel cell car has a hydrogen storage tank. The hydrogen gas must be compressed at extremely high pressure of 5,000 to 10,000 pounds per square inch (psi) to store enough fuel to obtain adequate driving range (Natural Gas Vehicles for America, www, 2011),

3. motor: it governs flow of electricity in the vehicle. By drawing power from either the battery or the fuel cell stack, it delivers electric power to the motor, which then uses the electricity to drive the vehicle (U.S. DOE, Office of EERE, Alternative & Advanced Vehicles, www, 2010), and

4. battery: fuel cell car has a battery that stores electricity generated, which increase the overall efficiency of the vehicle (U.S. DOE, Office of EERE, Alternative & Advanced Vehicles, www, 2010).

1.3 Fuel cells

A fuel cell is a device that generates electricity by an electrochemical reaction. A single fuel cell has two electrodes (anode and cathode), an electrolyte, and a catalyst. In practice, many fuel cells are usually assembled into a stack for more electricity production. There are several different types of fuel cells, typically grouped according to their operating temperatures and types of electrolytes used (Table 1.1). The amount of power generated by a fuel cell is determined by several factors

including fuel cell types, size, operating temperatures, and pressure. The most common type of fuel cell used in fuel cell car is proton exchange membrane fuel cell (PEMFC).

Table 1.1 Comparisons of fuel cell technologies applications (Carrette *et al*., 2001).

Fuel cell types	Electrolytes	Operating temperatures (°C)	Applications
Proton exchange membrane fuel cell (PEMFC)	Polymer	50-100	- Backup power - Portable power - Transportation
Alkaline fuel cell (AFC)	KOH	90-100	- Military, Space
Phosphoric acid fuel cell (PAFC)	H_3PO_4	150-200	- Distributed generation
Solid oxide fuel cell (SOFC)	ZrO_2	700-1000	- Auxiliary power - Electric utility - Distributed generation
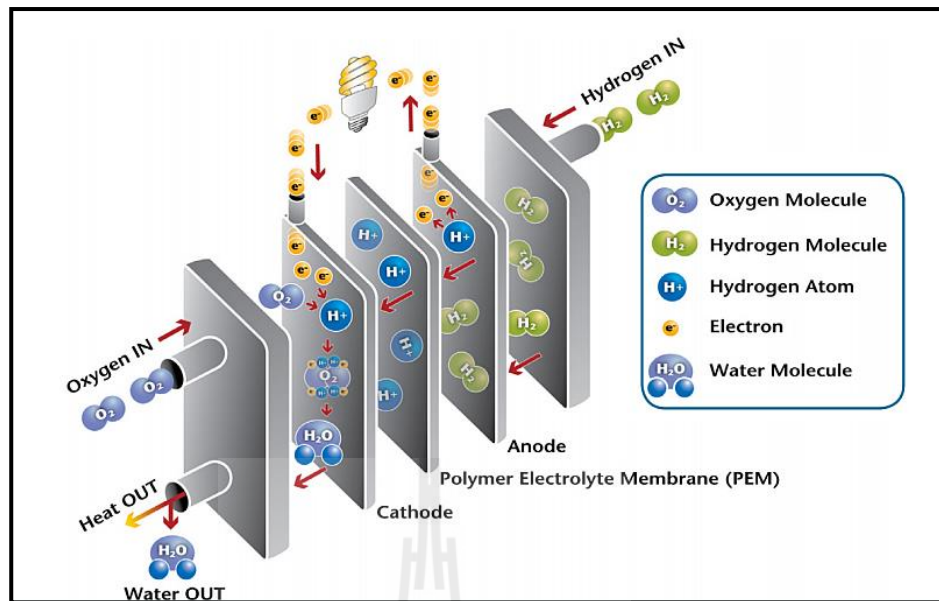
Figure 1.2 PEMFC single cell (http://energydesignresources.com/resources/e-news/e-news-90-fuel-cells.aspx).

Considering reaction mechanisms of PEMFC, the anode interacts with the provided fuel source hydrogen gas to generate protons and electrons. The protons travel through the electrolyte membrane to the cathode, while the electrons, which cannot pass through the electrolyte, create the electric current before being returned to cathode. The cathode then catalyzes oxygen with protons and returned electrons, and this combination produces water and heat as products. The reaction mechanisms of PEMFC are shown in the following equations.

$$\text{Anode:} \qquad 2H_2 \rightarrow 4H^+ + 4e^- \tag{1}$$

$$\text{Cathode:} \qquad O_2 + 4H^+ + 4e^- \rightarrow 2H_2O + \Delta \tag{2}$$

$$\text{Overall:} \qquad 2H_2 + O_2 \rightarrow 2H_2O + \Delta \tag{3}$$
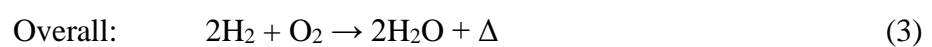
PEMFC is a type of low temperature fuel cell with an operating temperature in the range of 50-100 °C. Moreover, it has high current density and power density. When compared to other fuel cells, PEMFC has compact design, light weight, and faster response time. For practical uses in fuel cell car, many single PEMFCs are usually combined as a fuel cell stack. Furthermore, to use PEMFC stack efficiently, effective on-board hydrogen storages with high capacity (both gravimetric and volumetric storage) as well as operating at moderate temperature conditions are extremely required.

1.4 Hydrogen storage methods

In principle, hydrogen can be stored in many forms, mainly as compressed hydrogen gas, liquid hydrogen, and solid state hydrides (Table 1.2).

Table 1.2 Comparison of three major competing technologies for hydrogen storages (Varin *et al.*, 2009).

Storage systems	Volumetric hydrogen capacity ($kgH_2 \ m^{-3}$)	Drawbacks
Compressed hydrogen gas under 80 MPa pressure	~40	- safety problem - cost of pressurization - large pressure drop during use
Liquid hydrogen at cryogenic tank at -252 °C (21 K)	~71	- large thermal losses (open system) - safety problem - cost of liquefaction
Solid state hydrides	80-160	- none of the above

1.4.1 Compressed hydrogen gas

For this system, hydrogen is normally compressed and stored in gas cylinders, which are the simplest and cheapest method for on-board vehicles. However, its main obstacle is low storage density. In addition, high storage pressures raise the cost of the system as well as safety issues (Sandi, 2004)**.**
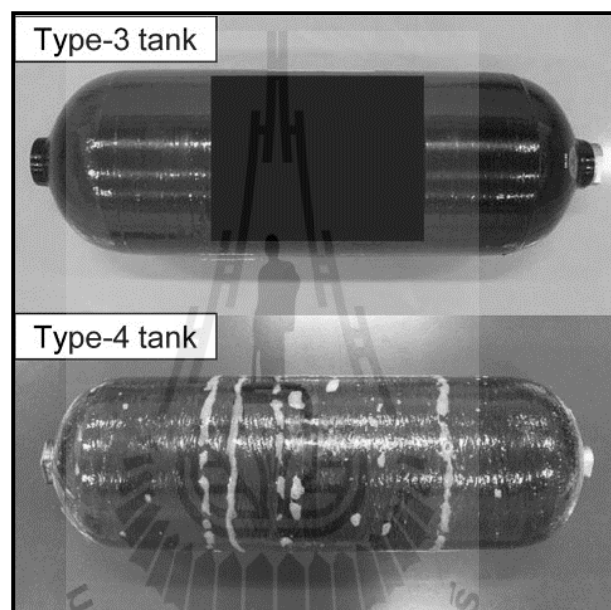
Figure 1.3 Compressed hydrogen gas tank (Tomioka *et al*., 2011).

1.4.2 Liquid hydrogen

Liquid hydrogen is an alternative storage to compressed hydrogen, where hydrogen can be liquefied under critical low temperature (-252 °C). Liquefaction takes place through a number of steps, in which the hydrogen is compressed and cooled to form a dense liquid. A major drawback of liquefied hydrogen storage is high cost of liquefaction processes and huge amount of electricity consumption (Züttel, 2004).
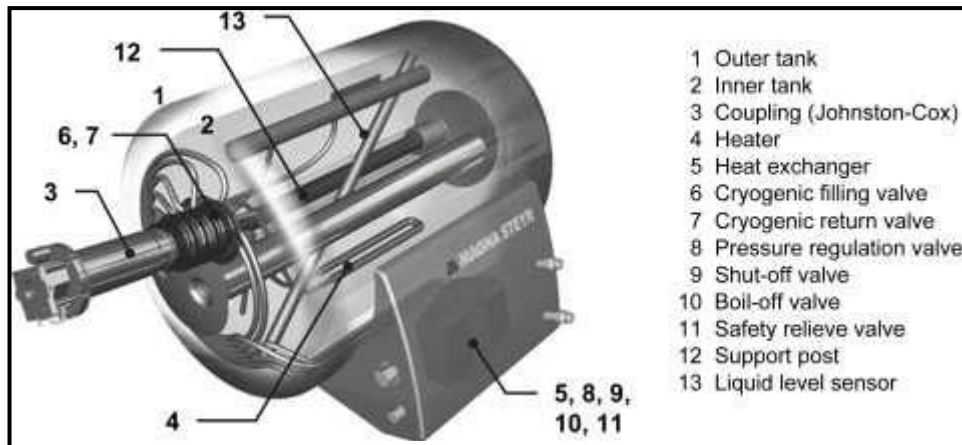
Figure 1.4 Liquid hydrogen tank (Mori *et al*., 2009).

1.4.3 Solid state hydrides

In solid state hydrides, hydrogen can be stored by combining hydrogen with solid state materials through chemical reactions. Many metals are able to be combined chemically with hydrogen to form a class of compounds called metal hydrides. Metal hydrides have the highest volumetric hydrogen density and operate without drawbacks as in compressed and liquid hydrogen systems. Moreover, the storage tank is compact with respect to those of compressed and liquid hydrogen (Basic Research Challenges for Hydrogen Storage, 2004).

Figure 1.5 Solid state hydrogen storage tank (http://www.flyhy.eu/HZG.html).

Therefore, several research groups have focused on solid state hydrides for hydrogen storage applications. However, there are still a lot of obstacles needed to be solved, especially high temperature of hydrogen sorption and slow kinetics. The targets for hydrogen storage materials mentioned by Department of Energy (US DOE) in 2015 are reviewed by Varin *et al*. (2009) and shown in Table 1.3.

Table 1.3 US DOE Freedom CAR hydrogen storage system targets (Varin *et al*., 2009).

Targets	2015
Specific energy (MJ kg^{-1})	10.8
Gravimetric capacity (wt.%)	9
Volumetric capacity (kgH$_2$ m^{-3})	81
Storage system cost ($ per kgH$_2$)	67
Operating temperature (°C)	-40/60
Cycle life-time (absorption/desorption cycles)	1,500

CHAPTER II

LITERATURE REVIEWS

Among all hydrogen storage materials, solid state hydrides have the highest hydrogen volumetric and gravimetric densities, and they do not need excessively high pressure and low temperature as required for compressed gas and liquid hydrogen. Moreover, the solid state hydrides have been proposed to be one of the most suitable on-board H_2 storages in transportation applications powered by PEMFC stack due to its high volumetric hydrogen capacity of 80-160 kgH_2 m^{-3}, compact size, light weight, and high purity of H_2 output (Varin *et al*., 2009; Schlapbach and Züttel, 2001; Ritter *et al*., 2003; Züttel *et al*., 2003; Fichtner *et al*., 2005). These solid state H_2 storage materials are reported in several forms, e.g., metal hydrides (MgH_2 and AlH_3) (Bogdanovic and Schwickardi, 1997), complex hydrides ($LiAlH_4$, $Mg(AlH_4)_2$, $NaAlH_4$, Na_3AlH_6, Na_2LiAlH_6) (Sun *et al.*, 2003; Fu *et al.*, 2006), and composite hydrides ($LiBH_4$-$NaAlH_4$) (Gross *et al*., 2008; Rongeata *et al.*, 2010).
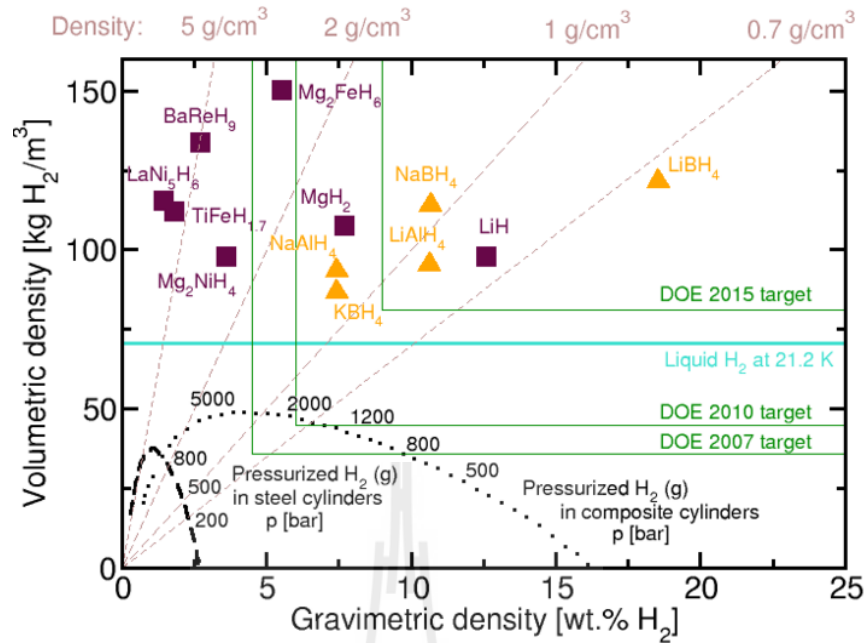
Figure 2.1 Volumetric and gravimetric hydrogen storage densities of different hydrogen storages (Grochala and Edwards, 2004).

From Figure 2.1, metal hydrides are represented by squares and complex hydrides triangles. Among them, lithium borohydride ($LiBH_4$) is one of the most outstanding complex hydrides because of its high volumetric and gravimetric hydrogen storage capacities (Züttel *et al*., 2003). Unfortunately, its practical application in mobile fuel cell systems is limited due to both thermodynamic and kinetic drawbacks. It was found that after melting at about 280 °C, $LiBH_4$ started to dehydrogenate slowly (above 400 °C) to form LiH, B, and H_2 as shown in the following equation.

$$LiBH_4 \rightarrow LiH + B + 3/2H_2 \qquad (13.8 \text{ wt.\% } H_2) \qquad (4)$$

For rehydrogenation, it remains difficult due to the inactive elemental boron, resulting in very high operating temperature (above 600 °C) and pressure (350 bar H_2) required (Aoki *et al*., 2005).

Moreover, sodium aluminium hydride ($NaAlH_4$), which has gravimetric and volumetric hydrogen storage capacities of 7.6 wt.% H_2 and 94 kgH_2 m^{-3}, respectively, is regarded as one of the most promising compounds for H_2 storage material (Bogdanovic and Schwichardi, 1997). The dehydrogenation and hydrogenation of $NaAlH_4$ occur according to the following equations:

$$NaAlH_4 \leftrightarrow 1/3Na_3AlH_6 + 2/3Al + 3/2H_2 \quad (3.7 \text{ wt.\% } H_2) \tag{5}$$

$$Na_3AlH_6 \leftrightarrow 3NaH + Al + 3/2H_2 \quad\quad (1.9 \text{ wt.\% } H_2) \tag{6}$$

$$NaH \rightarrow Na + 1/2H_2 \quad\quad\quad\quad (1.9 \text{ wt.\% } H_2) \tag{7}$$
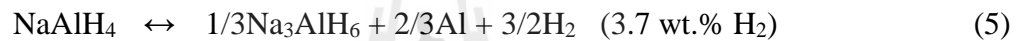
In theory, the first and the second steps released 3.7 and 1.9 wt.% H_2 at temperature of 274 and 299 °C, respectively (equations (5) and (6)). The last step released 1.9 wt.% H_2, which occurred in the temperature range of 425-500 °C (equation (7)). For the last step, the decomposition of NaH required high temperature is not useful for PEMFC. Therefore, the practical H_2 capacity is only 5.7 wt.%. Moreover, the reversibility was achieved only under high temperature (150 °C) and pressure (100 bar H_2) conditions (Bogdanovic *et al*., 2006). From the disadvantages of $LiBH_4$ and $NaAlH_4$, there are various methods including catalytic doping, composite hydrides, and nanoconfinement in nanoporous scaffolds, proposed to decrease dehydrogenation temperature and to increase reversible reaction kinetics of $LiBH_4$ and $NaAlH_4$.

2.1 Catalytic doping

Yang *et al*. (2007) reported the destabilization of LiBH$_4$ by doping with metals (Mg, Al, Ti, V, Cr, or Sc) or metal hydrides (MgH$_2$, TiH$_2$, or CaH$_2$). They found that all LiBH$_4$ composites with metals and metal hydrides showed lower desorption temperature than pure LiBH$_4$ and LiBH$_4$ mixed with MgH$_2$ presented the lowest desorption temperature. Xia *et al*. (2009) enhanced the hydrogen storage properties of LiBH$_4$ by ball milling with various ratios of Ni powder, i.e., 2:1, 4:1 and 6:1 (LiBH$_4$:Ni molar ratio) (Figure 2.2).
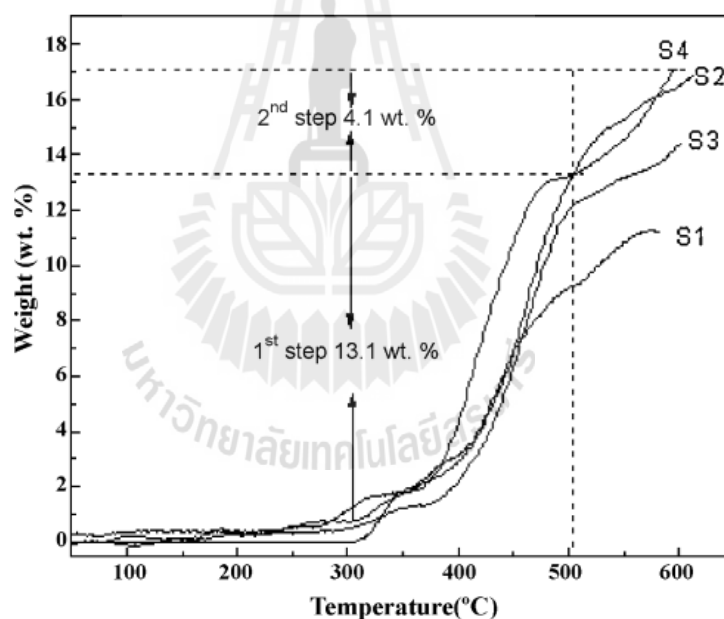
Figure 2.2 Hydrogen desorption curves of pure LiBH$_4$ (S1) and LiBH$_4$–Ni with LiBH$_4$:Ni molar ratios of 2:1 (S2), 4:1 (S3) and 6:1 (S4) (Xia *et al*., 2009).

From Figure 2.2, the dehydrogenation of LiBH$_4$ and LiBH$_4$–Ni samples starts at approximately 300 °C, suggesting that the addition of Ni did not reduce the dehydrogenation temperature of LiBH$_4$. However, at about 600 °C, the weight loss

from S2, S3 and S4 samples are 17.2, 14.4 and 16.5 wt.% H_2, respectively, which are higher than that of pure $LiBH_4$ (11 wt.% H_2). Furthermore, the rehydrogenation of $LiBH_4$-Ni systems could be reversible partially at 600 °C under 100 bar H_2, where the operating condition is milder than pure $LiBH_4$ (600 °C, 350 bar H_2).

In the case of $NaAlH_4$, Bogdanovic *et al*. (2000) showed that the decomposition of $NaAlH_4$ could be kinetically enhanced and reversible with the addition of Ti-dopants. They found that addition of the Ti-dopants to $NaAlH_4$ enhanced the rate of reaction by decreasing the activation energy of the absorption and desorption cycles; however, the change in composition formation with the addition of Ti occurred in this material was still unknown. Sun *et al*. (2002) studied X-ray diffraction of $NaAlH_4$ doped with Ti-based dopants and they found that Ti^{3+} probably substituted Na^+ of bulk $NaAlH_4$, resulting in induced distortions of the lattice.

2.2 Composite hydrides

A typical example for destabilization of $LiBH_4$ is the composite hydrides. Shi *et al*. (2008) investigated the hydrogen storage properties of $LiBH_4$-$NaAlH_4$ composite, both undoped and doped with a $TiCl_3$ additive. They found that milled $2LiBH_4$–$3NaAlH_4$ doped with $TiCl_3$ gave a significant lower hydrogen release temperature as compared with undoped system. In the doped systems, the reaction between $LiBH_4$ and $NaAlH_4$ resulted in the formations of $LiAlH_4$ and $NaBH_4$. $LiAlH_4$ released hydrogen already at room temperature to form Li_3AlH_6, while $NaBH_4$ was destabilized by oxide-free Al at higher temperatures, which led to decrease of desorption temperature. In addition, the excess of $NaAlH_4$ could produce $LiNa_2AlH_6$ phase, which could be reversibly discharged and recharged hydrogen at 80 bar and 180 °C. In 2009, Blanchard *et al*. modified the reversibility of $LiBH_4$ by ball-milling

with $LiAlH_4$. $LiAlH_4$ could reduce the hydrogen desorption temperature of $LiBH_4$. For instance, the decomposition of $LiBH_4+LiAlH_4$ started at 100 °C and ended at 500 °C, which was lower than pure $LiBH_4$ (starting at 360 °C and ending at 500 °C). Later, Yu *et al*. (2009) investigated de/rehydrogenation mechanisms of $LiBH_4$ destabilized with metallic Al. They found that $LiBH_4$/Al mixture decomposed in two steps as the following reactions:

$$2LiBH_4 + Al \rightarrow 2LiH + AlB_2 + 3H_2 \qquad (8)$$
$$2LiH + 2Al \rightarrow 2AlLi + H_2 \qquad (9)$$
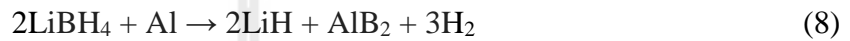
From reaction (8), AlB_2 was formed in the dehydrogenated state and disappeared in the hydrogenated state. The formation of AlB_2 decreased the stability of the materials, resulting in lower desorption temperature. Furthermore, rehydrogenation experiments revealed that an intermediate hydride was formed firstly at 600 °C and 30 bar H_2 pressure, and $LiBH_4$ could be reformed completely when H_2 pressure was increased to 100 bar. Zhang *et al*. (2009) improved the reversibility of $LiBH_4$ by synthesis of $LiBH_4–MgH_2–Al$ (4:1:1 molar ratio) composite. They found that the onset dehydrogenation temperature of $4LiBH_4–MgH_2–Al$ was reduced by 173 °C as compared with those of $2LiBH_4–MgH_2$ and $2LiBH_4–Al$ systems.
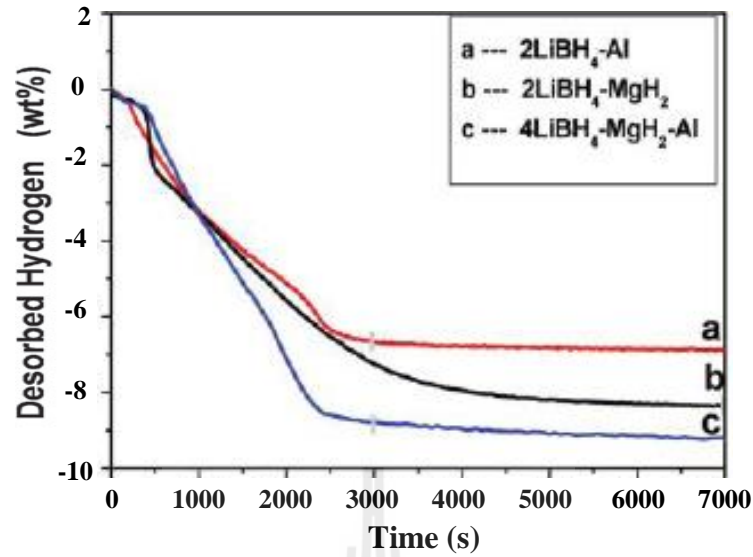
Figure 2.3 Isothermal dehydrogenation kinetics of $4LiBH_4$–MgH_2–Al, $2LiBH_4$–MgH_2, and $2LiBH_4$–Al systems under a background pressure of 0.01 bar H_2 and at 400 °C. (Zhang *et al*., 2009).

From Figure 2.3, at 3000 s, $4LiBH_4$–MgH_2–Al system releases hydrogen of 9.4 wt.%, approaching to theoretical value (9.9 wt.% H_2), while those of the $2LiBH_4$–MgH_2 and $2LiBH_4$–Al samples are 8 and 6.5 wt.% H_2, respectively. The dehydrogenation reaction mechanism of $4LiBH_4$–MgH_2–Al composite was proposed as shown in the following reaction:

$$4LiBH_4 + MgH_2 + Al \rightarrow 4LiH + MgAlB_4 + 7H_2 \tag{10}$$

As shown in reaction (10), the additions of MgH_2 and Al could effectively inhibit the formation of elemental boron during dehydrogenation ($MgAlB_4$ instead). For the rehydrogenation reaction of LiH–$MgAlB_4$, it occurred in two steps as $4LiH + MgAlB_4 + 6H_2 \rightarrow Mg + 4LiBH_4 + Al$ and $Mg + H_2 \rightarrow MgH_2$. However, MgH_2 in the second step could not be fully recovered because partial Mg forming in the first step could alloy with Al to form Mg_2Al_3. Next, Vajo *et al*. (2010) investigated thermodynamic

and kinetic destabilization of $LiBH_4$ by addition of Mg_2NiH_4. They found that the equilibrium hydrogen pressure was higher than that of either pure $LiBH_4$ or pure Mg_2NiH_4, and it approached to ideal value for hydrogen storage in PEMFC applications. Moreover, onset dehydrogenation temperature of $LiBH_4$–Mg_2NiH_4 composite was lower than those of $LiBH_4$ and Mg_2NiH_4 individually, illustrating a new pathway enabled by the mixture (reaction (11)).

$$4LiBH_4 - 5Mg_2NiH_4 \leftrightarrow 2MgNi_{2.5}B_2 + 4LiH + 8MgH_2 + 8H_2 \qquad (11)$$
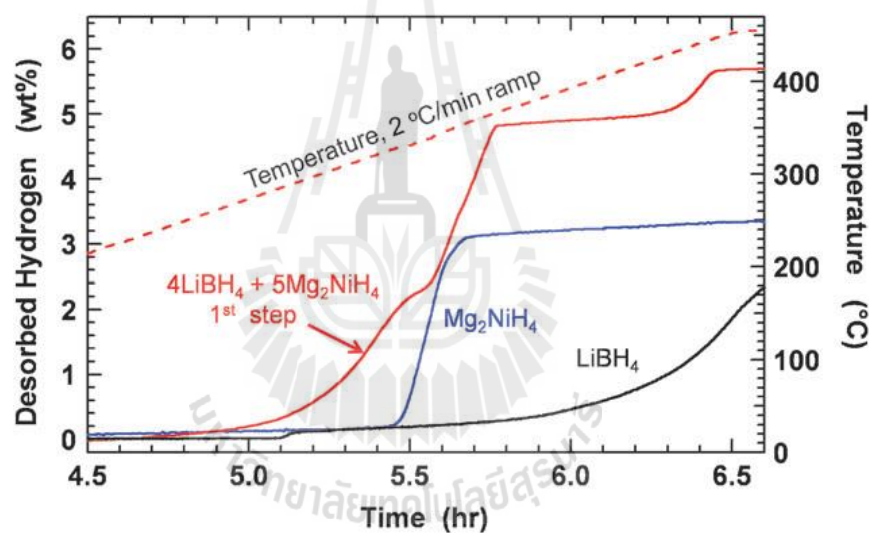
Figure 2.4 Dehydrogenation kinetics of $4LiBH_4$–$5Mg_2NiH_4$, Mg_2NiH_4, and $LiBH_4$ (Vajo *et al*., 2010).

From Figure 2.4, the dehydrogenation of $4LiBH_4$–$5Mg_2NiH_4$ occurs three steps at 250 °C, 340 °C, and 425 °C respectively. The amount of hydrogen desorbed in the 1st step is consistent with the reaction (11), which theoretically releases 2.6 wt.% H_2. The 2nd step corresponds to dehydrogenation of MgH_2 produced during the reaction between $LiBH_4$ and $MgNiH_4$ (reaction (11)) and the 3rd step is due to the decomposition of

excess LiBH$_4$ (Figure 2.4). Moreover, Dorthe *et al*. (2010) studied the hydrogen release of LiBH$_4$-NaAlH$_4$ composite.
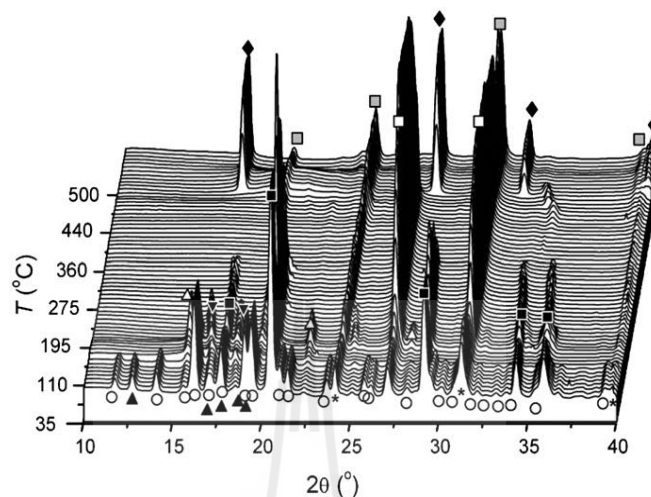
Figure 2.5 In situ SR-PXD data for the dehydrogenation of LiBH$_4$–NaAlH$_4$: ○ LiAlH$_4$, ■ NaBH$_4$, ▲ *o*-LiBH$_4$, ▼ *h*-LiBH$_4$, △ Li$_3$AlH$_6$, □ Al+LiH, ◪ AlB$_2$, ◆ LiAl, and *TiB$_2$ (Dorthe *et al*., 2010).

From Figure 2.5, the formation of AlB$_2$ is observed about 450 °C, which destabilizes boron and may be optimized to eliminate the release of diboran (B$_2$H$_6$). The pressure for dehydrogenation is reduced by the formation of LiAl. Moreover, the rehydrogenation of LiBH$_4$–NaAlH$_4$ composite could be reversible partially at 400 °C under 110 bar H$_2$, where the operating condition was milder than pure LiBH$_4$ (600 °C, 350 bar H$_2$).

2.3 Nanoconfinement in nanoporous scaffolds

Further approach to improve de/rehydrogenation kinetics is confinement of light metal hydrides in nanoporous scaffolds. Zhang *et al*. (2007) reported that LiBH$_4$ nanoparticles supported by disordered mesoporous carbon CMK-3 showed favorable

latent heat of dehydrogenation (40 kJ/mol H_2), large amount of dehydrogenation capacity (14 wt.% H_2) below 600 °C, and reversible capacity of 6.0 wt.% H_2 at 350 °C. Gross *et al*. (2008) demonstrated that the desorption temperature of $LiBH_4$ was lowered by 75 °C and the dehydrogenation rate at 300 °C increased up to 50 times, when $LiBH_4$ was incorporated into nanoporous structure of carbon scaffold. Furthermore, nanoconfined $LiBH_4$ showed a reversible hydrogen uptake (75 % of original capacity) at relatively mild conditions of 100 bar H_2, 400 °C for 2 h. Next, Liu *et al.* (2010) investigated the wetting and decomposition behavior of $LiBH_4$ in the presence of highly ordered nanoporous hard carbon (NPC) with hexagonally packed (2 nm diameter columnar pores). The confinement of $LiBH_4$ in small pores showed low temperatures of phase transition and melting of $LiBH_4$ as well as the significant decrease of the onset desorption temperature with respect to bulk $LiBH_4$. Most significantly, their results suggested that diborane release was suppressed during the decomposition of nanoconfined $LiBH_4$. For nanoconfined $NaAlH_4$, Nielsen *et al*. (2014) studied nanoconfined $NaAlH_4$ in nanoporous scaffolds with different surface areas, pore volumes, and pore sizes. Carbon aerogel scaffold (CAS) was obtained by pyrolyzing at 950 °C under CO_2 flow (CO_2-activated CAS). They found that by using CO_2-activated technique surface area and pore volume of CAS were significantly increased as compared with that prepared by using N_2 as flowed gas. The content of $NaAlH_4$ melt infiltrated into CO_2-activated CAS was up to 91 mol%, significantly higher than that into CAS prepared by using N_2-flowed gas (52 mol%). Furthermore, the stability of nanoconfined $NaAlH_4$ over several cycles of hydrogen release and uptake was significantly improved by the CO_2-activated CAS due to interaction between $NaAlH_4$ and CAS. However, the disadvantages of nanoconfinement in

nanoporous carbon scaffolds are high operating pressure and temperature for de/rehydrogenation as well as oxidation of metal hydrides. Therefore, new host materials for nanoconfinement are expected not only to reduce pressure and temperature for de/rehydrogenation, but also to prevent metal hydrides from air and humidity.

Interestingly, Jeon *et al*. (2011) reported the synthesis of an air-stable composite material consisting of Mg nanocrystals (NCs) in poly (methyl methacrylate) (PMMA). PMMA shows high permeability ratio of H_2/O_2 (ratio of 42.9 at 35 °C). In this work, PMMA was used to keep Mg away from water and oxygen but let hydrogen in or out freely (Wang *et al*., 2008; Liang *et al*., 2011; Mark, 1999). They found that the sample could absorb 5.97 wt.% H_2 at 200 °C under 35 bar H_2 within 80 min, while Mg powder could not absorb hydrogen in the same condition. Moreover, prevention of Mg nanoparticles from deterioration by oxygen and water was obtained by embedding in PMMA (Figure 2.6).
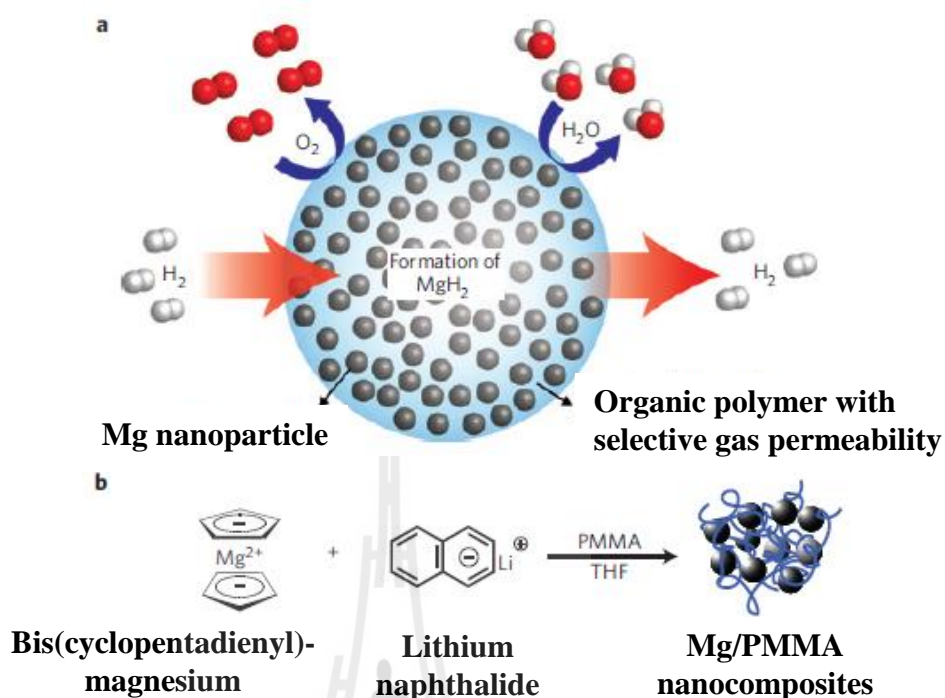
Figure 2.6 Mg NCs in a gas-barrier PMMA polymer matrix (Jeon *et al*., 2011).

Next, Huang *et al*. (2014) investigated the dehydrogenation temperature of LiBH$_4$ compositing with poly (methyl methacrylate) (PMMA). They found that interaction between LiBH$_4$ and PMMA led to fast H$_2$ release at low temperature. Meanwhile, PMMA not only can protect LiBH$_4$ from water and oxygen, but also let hydrogen in and out freely. LiBH$_4$ composited with PMMA started to dehydrogenate at 53 °C and released 5.2 wt.% H$_2$ at 162 °C within 1 h. It could be concluded that PMMA could prevent deterioration of LiBH$_4$ in the atmosphere and could reduce its dehydrogenation temperature.

Recently, Gosalawit-Utke *et al*. (2014) destabilized LiBH$_4$ by nanoconfinement in poly (methyl methacrylate)-co-butyl methacrylate (PcB) polymer matrix. On the basis of a butyl-branched chain, PcB has a superior amorphous degree as compared to PMMA, leading to higher free volume in the polymer matrix for H$_2$

permeability. They found that the onset dehydrogenation temperature of nanoconfined LiBH$_4$ in PcB was ~80 °C and it released 0.74 wt.% H$_2$ (8.8 wt.% H$_2$ with respect to LiBH$_4$ content) at 120 °C under vacuum within 4 h during the 1st dehydrogenation. Furthermore, the nanoconfined LiBH$_4$–PcB could be rehydrogenated at mild condition of 140 °C under 50 bar H$_2$ for 12 h. However, the disadvantages of nanoconfined LiBH$_4$–PcB are LiBH$_4$/PcB interaction between boron (B) of LiBH$_4$ with metoxy (–OCH$_3$) group of PcB and partial thermal degradation of PcB polymer, resulting in the reduction of H$_2$ content release and uptake.

Therefore, in this work, we doped small amount of NaAlH$_4$ in nanoconfined LiBH$_4$–PcB. NaAlH$_4$ is expected to decrease LiBH$_4$/PcB interaction and improve thermal stability of PcB host by providing competitive interaction with PcB.

2.4 Research objectives

2.5.1   To prepare NaAlH$_4$ doped into nanoconfined LiBH$_4$–PcB.

2.5.2   To study kinetic properties of nanoconfined LiBH$_4$–PcB samples with and without NaAlH$_4$.

2.5.3   To reduce LiBH$_4$/PcB interaction and to improve thermal stability of PcB.

CHAPTER III

EXPERIMENT

3.1 Chemicals and materials

Poly (methyl methacrylate)-co-butyl methacrylate (PcB, MW = 75,000), 2 M lithium borohydride solution in THF (LiBH$_4$, ≥90%, hydrogen storage grade), and sodium aluminium hydride (NaAlH$_4$, ≥93%, hydrogen storage grade) were purchased from Sigma-Aldrich (St. Louis, MN, USA). Tetrahydrofuran (THF, HPLC grade) and n-hexane (AR grade) were purchased from QRëC^{TM}. Metallic sodium (Na) and benzophenone ((C$_6$H$_5$)$_2$CO) were purchased from Fluka chemika (Buchs, Switzerland).

3.2 Sample preparations

3.2.1 Purification of tetrahydrofuran

THF was pre–dried overnight by molecular sieves. Metallic Na and benzophenone of 5 and 20 g, respectively, were added to 500 mL of pre-dried THF (Schwartz, 1978). The mixture was refluxed under nitrogen atmosphere at 80 °C until a deep blue color was obtained. The mixture was distilled at 70 °C under nitrogen atmosphere to obtain anhydrous THF.

3.2.2 Precipitation of PcB

PcB of 20.4890 g was dissolved in 100 mL anhydrous THF with continuous stirring to obtain homogeneous polymer solution (20.0 %w/v). The PcB polymer

solution was precipitated in distilled n-hexane and dried at 90 °C for 24 h in vacuum oven to obtain dried PcB polymer powder.

3.2.3 Dissolving of NaAlH₄ in anhydrous tetrahydrofuran

NaAlH₄ powder of 0.3013 g was dissolved in 85 mL anhydrous THF and continuously stirred for several hours in the glove box to obtain NaAlH₄ solution (0.35 %w/v NaAlH₄ in THF).

3.2.4 Synthesis of nanoconfined LiBH₄ in PcB

The polymer solution was prepared by dissolving 5.0656 g of PcB in 20 mL anhydrous THF with continuous stirring. LiBH₄ solution of 15 mL was added into PcB polymer solution with continuous stirring under argon atmosphere in the glove box. The transparent gel was obtained after stirring the mixture of LiBH₄ and PcB for approximately 10 min. The LiBH₄−PcB gel was dried in the glove box to achieve the powder sample, containing 11.5 wt.% of LiBH₄, denoted as nano LiBH₄−PcB. With respect to the LiBH₄ content, theoretical hydrogen storage capacity of 1.60 wt.% was achieved.

3.2.5 Synthesis of nanoconfined LiBH₄−NaAlH₄ in PcB

PcB powder of 0.5144 g was dissolved in 5 mL anhydrous THF to obtain PcB polymer solution. The solutions of LiBH₄ and NaAlH₄ of 1.5 and 2 mL, respectively, were added into PcB polymer solution. The mixture was stirred for 1 h until transparent gel was achieved. The transparent gel was dried at room temperature in the glove box for several days to obtain nano LiBH₄−NaAlH₄−PcB powder sample, where the molar ratio of LiBH₄:NaAlH₄ was 10:0.5. The sample contained 11.2 and 1.2 wt.% of LiBH₄ and NaAlH₄, respectively. Due to small amount of NaAlH₄ doped,

it was considered as an additive, where H_2 storage capacity could be negligible. Thus, with respect to $LiBH_4$ content, theoretical hydrogen storage capacity of nano $LiBH_4-NaAlH_4-PcB$ was calculated to be 1.55 wt.%.

3.3 Characterizations

3.3.1 Fourier transform infrared spectrometry (FTIR)

Fourier transform infrared (FTIR) spectra of standard samples ($NaAlH_4$, $LiBH_4$ and PcB) and nanoconfined samples of $LiBH_4-PcB$ and $LiBH_4-NaAlH_4-PcB$ were obtained by using a Bruker, IR spectrometer (Tensor 27). The sample was ground with anhydrous KBr (1:10 weight ratio of sample:anhydrous KBr) and pressed under 3 tons for 2 min to obtain KBr pellet. KBr pellet containing the sample was assembled in the FTIR machine on the direction of infrared. The spectrum was recorded in the range of 4000-400 cm^{-1} with 32 scans at room temperature. Quantitative analysis was done by curve fitting technique using Magic plot program.

3.3.2 Scanning electron microscopy (SEM)

Morphologies of the samples were obtained using scanning electron microscopy (SEM) (Zeiss, Auriga). Nano $LiBH_4-NaAlH_4-PcB$ powder sample was deposited on the sample holder by using silver glue (in *n*-butyl acetate). The powder sample was coated with platinum (Pt) by using a sputtering technique with a current of 30 mA for 30 s under vacuum. An energy-dispersive X-ray spectroscopy (EDS)-elemental mapping were managed by an apparatus from EDAX Inc., USA. Smart SEM and EDS Genesis programs were used for morphological studies and elemental analysis of the samples, respectively.

3.3.3 Kinetics measurement

De/rehydrogenation kinetics and hydrogen reproducibility of nano LiBH₄−PcB and nano LiBH₄−NaAlH₄−PcB were studied by using a laboratory scale setup of a Sievert–type apparatus (Figure 3.1) (Gosalawit–Utke *et al.*, 2014). The powder sample of ~50–100 mg was packed in a high pressure stainless steel sample holder (316SS, Swagelok) under argon atmosphere in the glove box, and transferred to the Sievert–type apparatus. Two K–type thermocouples (-250-1,300 °C, SL heater) were attached to the sample holder and to the furnace for measuring the temperature change of the system during de/rehydrogenation. Pressure transducers (C206, Cole Parmer) in the pressure range of 0-500 psig and 0-3000 psig were used to measure the pressure change due to hydrogen desorption and absorption, respectively. Thermocouples and pressure transducers were connected to an AI210I module convertor data logger (from Wisco), measuring and transferring (every 1 s) the pressure and temperature changes of the sample to the computer for further evaluation. The samples was dehydrogenated by heating from room temperature to 120 °C (5 °C/min) under vacuum. Temperature was controlled by a PID temperature controller. In the case of rehydrogenation, the dehydrogenated powder sample was pressurized under 60 bar H_2 (purity = 99.999 %) at 120 °C for 12 h. Once the pressure reading was constant over a period of time, the amount of hydrogen released was calculated by the pressure change (ΔP) and the following equations:

$$(\Delta P)V = nRT$$

$$H_2 \text{ desorbed (wt.\%)} = [(n \times 2.0158)/\text{sample weight}] \times 100$$

where *P*, *V*, and *T* are hydrogen pressure (atm), volume of the system (L), and temperature (K), respectively, *n* is the number of hydrogen moles (mol), and *R* is gas constant (0.0821 L atm K^{-1} mol^{-1}).
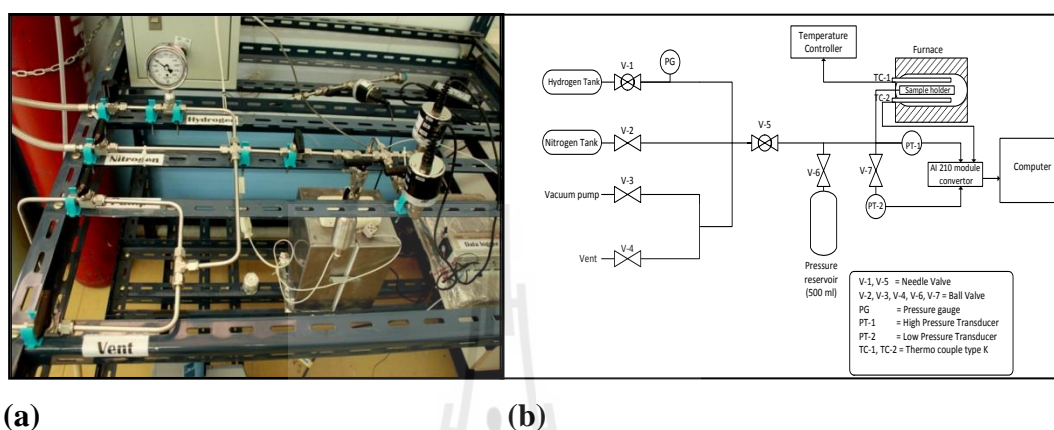
Figure 3.1 Picture (a) and schematic diagram (b) of Sievert-type apparatus.

3.3.4 X-ray photoelectron spectroscopy (XPS)

X-ray photoelectron spectroscopy was carried out at the Siam Photon Laboratory, BL3.2a in the Synchrotron Light Research Institute (Public Organization), Nakhon Ratchasima, Thailand. The powder samples of LiBH$_4$, nano LiBH$_4$−PcB, and nano LiBH$_4$–NaAlH$_4$–PcB were held on the sample holders by using carbon glue tape in the glove box atmosphere. Prior to the measurements, all prepared samples were placed in an ultrahigh vacuum chamber for approximately 6 h. The photon energy of 400 eV was used to detect the signals of Li 1*s* and B 1*s*. Each element was investigated at the kinetic energy step of 0.1 eV for 5 scans by using an CLAM2 analyzer. The multi spectra were analyzed by using a macro XPS MS Excel 2007 (Windows XP) software.

3.3.5 Nuclear magnetic resonance (NMR) measurement

Solid-state ^{11}B, ^{27}Al and ^{23}Na magic angle spinning (MAS) nuclear magnetic resonance (NMR) spectra of $LiBH_4$, $NaAlH_4$, and nano $LiBH_4$–$NaAlH_4$–PcB were recorded by a Bruker ASCEND^{TM} 500 spectrometer using a BL4 VNT probe for 4 mm outer diameter rotors. The powder sample was tightly packed in a zirconia end-capped tube in the glove box, and solid–state MAS NMR measurements were carried out at 302 K. Solid-state MAS NMR experiments employed a rotation frequency of 10 kHz. The excitation pulse lengths of ^{11}B and ^{27}Al MAS NMR were 5 and 9.8 μs, respectively. The relaxation delays of ^{11}B, ^{27}Al, and ^{23}Na MAS NMR were 5 s. The ^{11}B, ^{27}Al, and ^{23}Na chemical shifts were detected in part per million (ppm) relative to neat boric acid (H_2BO_3), aluminium oxide (Al_2O_3), and NaCl, respectively.

3.3.6 Powder X−ray diffraction (XRD) measurements

Powder X-ray diffraction patterns of PcB, nano $LiBH_4$ − PcB, and nano $LiBH_4$−$NaAlH_4$–PcB were obtained from a Bruker D8 Advance by using a CuK$_α$ ($λ$ = 0.15406 nm) radiation. The experiments were done in step scan mode with a step interval of 0.500°/s (40 mV and 40 mA) over the 2θ range of 10–80°. The powder sample was packed in a sample holder under argon atmosphere in the glove box and covered by a plastic dome made from PMMA.

3.3.7 Gas analysis

The analyses of gases released during dehydrogenation of nano $LiBH_4$–PcB and nano $LiBH_4$–$NaAlH_4$–PcB were carried out by connecting a manometric PCTPro– 2000 apparatus with a residual gas analyzer (RGA200, Setaram, France) by using a 1/8" stainless steel tube. The powder sample (~200 mg) was loaded in the sample

holder and transferred to the PCTPro–2000 apparatus. The measurement was done by heating the powder sample from room temperature to 300 °C (5 °C/min) under vacuum.
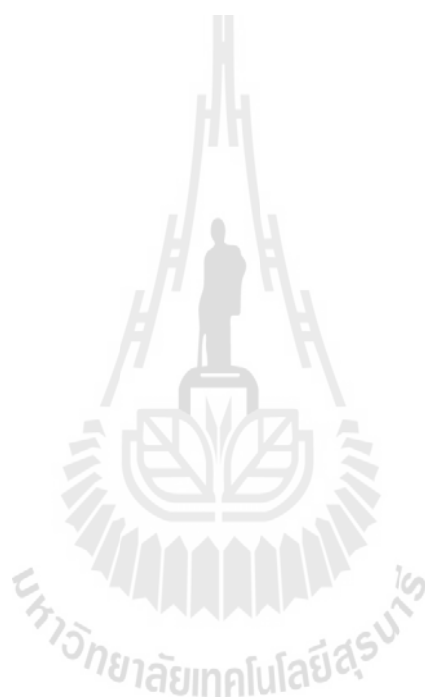
CHAPTER IV

RESULTS AND DISCUSSION

4.1 Dissolving of NaAlH$_4$ in anhydrous tetrahydrofuran

In order to confirm the successful dissolving of NaAlH$_4$ in THF, Fourier transform infrared spectrometer (FTIR) was used to characterize NaAlH$_4$ and dissolved NaAlH$_4$ in THF. NaAlH$_4$ exhibits characteristic vibrational peaks of [AlH$_4$]$^-$ stretching and bending at 1636 and 888 cm^{-1}, respectively, (Figure 4.1 (a)) corresponding to the FTIR spectrum of NaAlH$_4$ previously reported (Rafi *et al*., 2012). For dissolved NaAlH$_4$ in THF, all the characteristic peaks corresponding to NaAlH$_4$ are observed (Figure 4.1 (b)). This confirms successful dissolving of NaAlH$_4$ in THF.
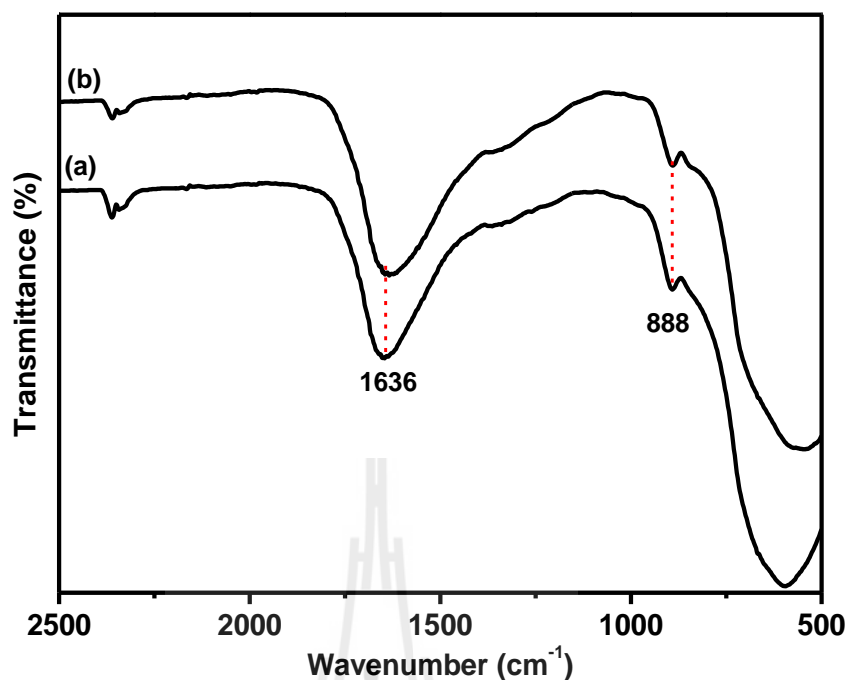
Figure 4.1 FTIR patterns of NaAlH$_4$ (a) and dissolved NaAlH$_4$ in THF (b).

4.2 Dispersion of LiBH$_4$ and NaAlH$_4$ in PcB polymer matrix

To investigate the dispersion of LiBH$_4$ and NaAlH$_4$ in PcB polymer matrix, SEM and EDS–mapping experiments of nano LiBH$_4$–NaAlH$_4$–PcB sample were done. Figure 4.2 (A) shows SEM image of nano LiBH$_4$−NaAlH$_4$–PcB and the elemental maps corresponding to the area depicted (Figures 4.2 (B-E)). From Figures 4.2 (B-E), good dispersion of carbon (C) from PcB, boron (B) from LiBH$_4$, and sodium (Na) and aluminium (Al) from NaAlH$_4$ are detected all over sample bulk. From Figure 4.2 (F), the signals of C and oxygen (O) from PcB are observed together with those of Na, Al, and B from NaAlH$_4$ and LiBH$_4$, respectively, as well as platinum (Pt) from surface coating. The missing of lithium (Li) signal from LiBH$_4$ can be due to the limitation of EDS technique to light element. From these results, it can be confirmed that LiBH$_4$ and NaAlH$_4$ are well dispersed into PcB polymer matrix.
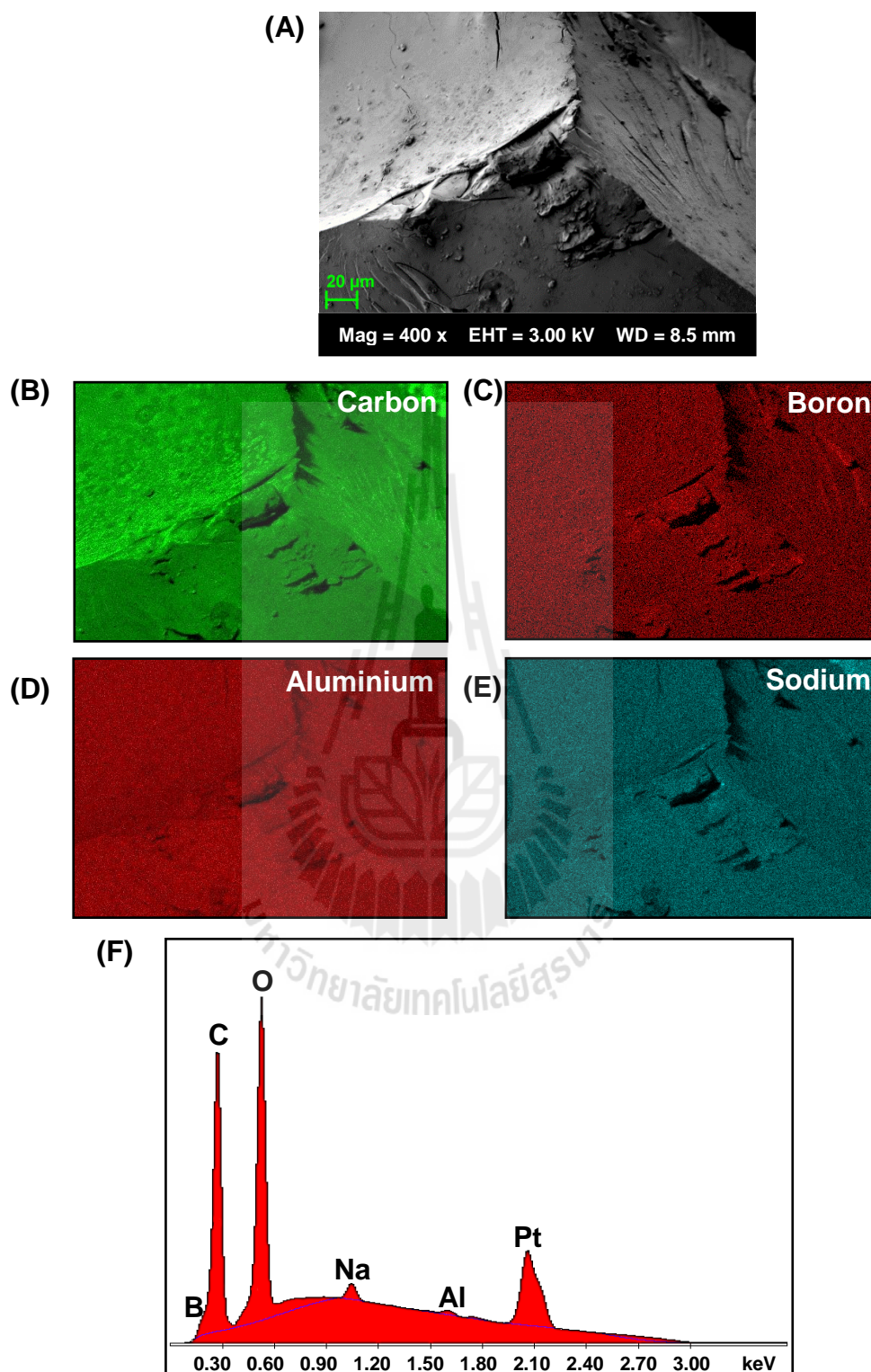
Figure 4.2 SEM image of nano LiBH$_4$−NaAlH$_4$−PcB (A), carbon mapping (B), boron mapping (C), aluminium mapping (D), sodium mapping (E), and quantitative elemental analysis (F).

4.3 Kinetic properties

To evaluate the performance of the hydrogen storage material, the storage capacity obtained from the sample must be compared with theoretical values. Theoretical hydrogen storage capacities of nanoconfined samples based on the amount of all components in the mixtures are calculated (Table 4.1). With respect to PcB polymer content in the samples, nano $LiBH_4$–PcB contains $LiBH_4$ of 11.5 wt.%, while nano $LiBH_4$–$NaAlH_4$–PcB consists of $LiBH_4$ and $NaAlH_4$ of 11.2 and 1.2 wt.%, respectively. On the basis of dehydrogenation of $LiBH_4$ (equation (4)), where 13.8 wt.% H_2 are theoretically released, the theoretical hydrogen storage capacity of the nano $LiBH_4$–PcB and nano $LiBH_4$–$NaAlH_4$–PcB are calculated to be 1.60 and 1.55 wt.%, respectively (Table 4.1).

Table 4.1 Amount of all components and theoretical hydrogen storage capacities of nanoconfined samples.

Nanoconfined samples	Amount of all components (wt.%)			Theoretical H_2 capacity (wt.%)
	PcB	LiBH$_4$	NaAlH$_4$	
LiBH$_4$–PcB	88.5	11.5	-	1.60
LiBH$_4$–NaAlH$_4$–PcB	87.6	11.2	1.2	1.55

To study the dehydrogenation kinetics, hydrogen release and uptake cycles of nano $LiBH_4$–PcB and nano $LiBH_4$–$NaAlH_4$–PcB were performed by using Sievert-type apparatus. Dehydrogenation and rehydrogenation were done at the same temperature of 120 °C under vacuum and 60 bar H_2, respectively. The amount of gases desorbed due to thermal degradation (at 120 °C under vacuum) of PcB polymer

matrix and NaAlH$_4$–PcB composite are 0.04 and 0.005 wt.%, respectively. Hydrogen

content released from nano LiBH$_4$–PcB and nano LiBH$_4$–NaAlH$_4$–PcB is obtained

from total amount of gas release subtracted with those of PcB and NaAlH$_4$–PcB

composite, respectively. From Figure 4.3 (A), the 1st dehydrogenation cycle of nano

LiBH$_4$–PcB releases 0.78 wt.% H$_2$ (49 % H$_2$ with respect to theoretical hydrogen

storage capacity) within 4 h. The inferior amount of H$_2$ released during 1st

dehydrogenation (0.78 wt.% H$_2$) with respect to theoretical value (1.60 wt.% H$_2$)

could be due to the interaction between LiBH$_4$ and PcB polymer chains (B---OCH$_3$),

discussed in the previous studies (Gosalawit–Utke *et al*., 2014). Afterwards, the

dehydrogenated sample from the 1st dehydrogenation was rehydrogenated at 120 °C

under 60 bar H$_2$ for 12 h. It results in desorbed hydrogen of only 0.32 wt.% H$_2$ during

the 2nd dehydrogenation (20 % H$_2$ with respect to theoretical hydrogen storage

capacity). The reduction of H$_2$ content released in the 2nd cycle with respect to the 1st

one could be due to the greater interaction between LiBH$_4$ and PcB after cycling and

thermal degradation of PcB polymer host during cycling under temperature and

pressure as previously discussed (Gosalawit–Utke *et al*., 2014). The latter leads to the

inferior nanoconfinement of LiBH$_4$ in PcB polymer matrix. Moreover, the higher the

interaction of LiBH$_4$/PcB (B---OCH$_3$), the lower the [BH$_4$]$^-$ content, resulting in the

lower H$_2$ storage capacity. In the case of nano LiBH$_4$−NaAlH$_4$−PcB, it exhibits H$_2$

desorption of 1.29 and 0.67 wt.% H$_2$ (83 and 43 % H$_2$ with respect to theoretical

hydrogen storage capacity, respectively) during the 1st and 2nd dehydrogenations,

respectively (Figure 4.3 (B)). It should be noted that nano LiBH$_4$−NaAlH$_4$−PcB

shows not only higher H$_2$ desorption content with respect to nano LiBH$_4$–PcB (the 1st

and 2nd cycles), but also faster desorption kinetics. For example, the dehydrogenation

of nano LiBH$_4$–NaAlH$_4$–PcB is completed within 1 h, while that of nano LiBH$_4$–PcB requires up to 4 h. Fast kinetics of nano LiBH$_4$–NaAlH$_4$−PcB could be due to the catalytic effects of NaAlH$_4$ on dehydrogenation of LiBH$_4$ (Shi *et al*., 2008).
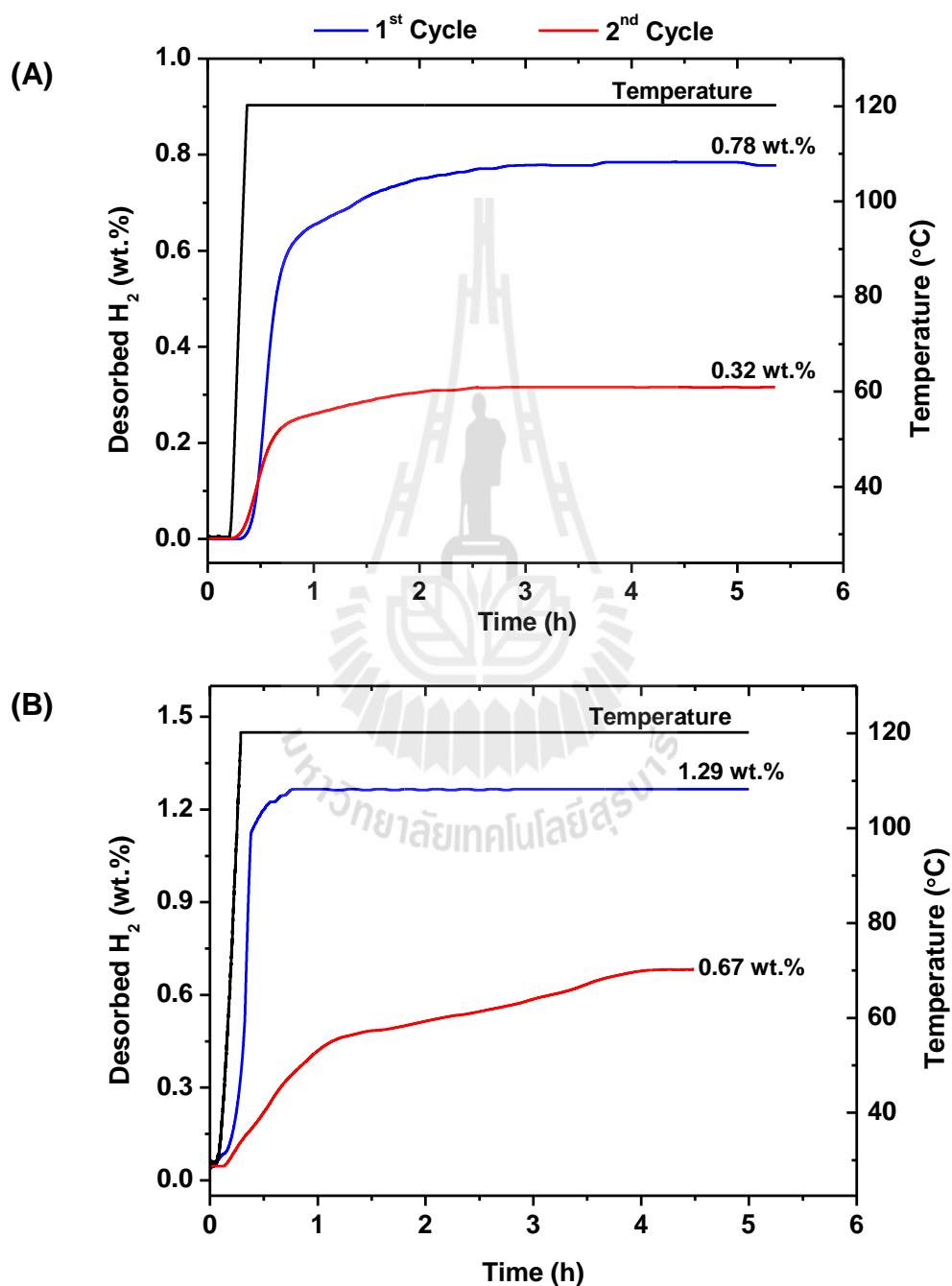
Figure 4.3 Hydrogen desorption 1st and 2nd cycles of nano LiBH$_4$−PcB (A) and nano LiBH$_4$–NaAlH$_4$–PcB (B).

4.4 Reversibility

In order to investigate the characteristics peak of reference materials and to study reversibility of nano LiBH$_4$−NaAlH$_4$–PcB, FTIR technique was used.
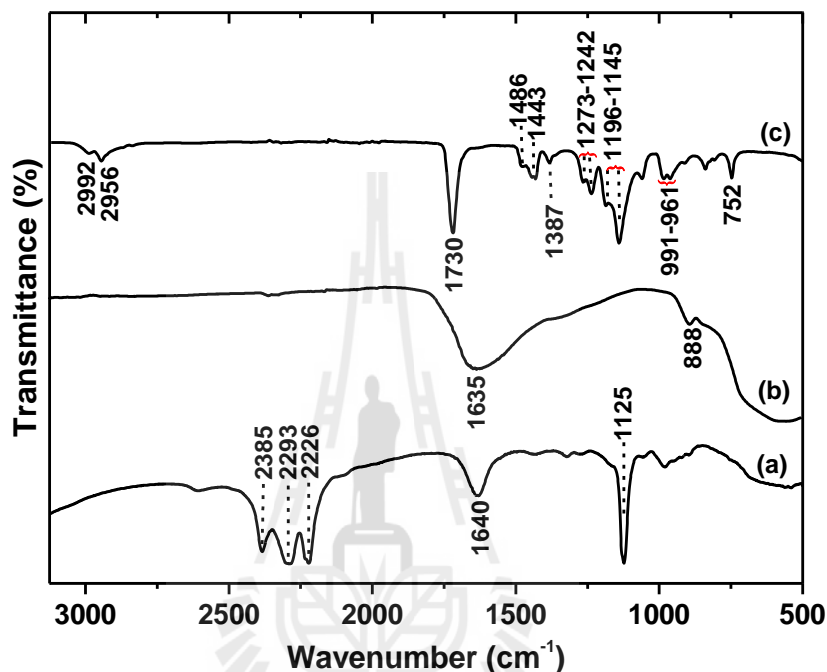
Figure 4.4 FTIR spectra of LiBH$_4$ (a), NaAlH$_4$ (b), and PcB (c).

For the reference materials, bulk LiBH$_4$ reveals the triplet peaks of B–H bond stretching at 2385, 2293, and 2226 cm^{-1}, while that of bending is at 1125 cm^{-1} (Figure 4.4 (a)). The peak at 1640 cm^{-1} refers to O−H bond from oxidation of LiBH$_4$ in ambient condition during the experiment (Yang *et al*., 2014). NaAlH$_4$ exhibits vibrational peaks of [AlH$_4$]$^-$ stretching and bending at 1635 and 888 cm^{-1}, respectively (Rafi *et al*., 2012) (Figure 4.4 (b)). For PcB, Figure 4.4 (c) shows a vibrational peak corresponding to C–H stretching at 2992–2956 cm^{-1} and C=O stretching of ester group at 1730 cm^{-1}. The vibrational peaks at about 1486 and 1443 cm^{-1} belong to asymmetric bending vibrations of (C–CH$_2$) and (C–CH$_3$) bonds, respectively. The two

peaks at 1387 and 752 cm⁻¹ are in accordance with α–methyl group vibration. The two

doublet bands at 1273–1242 and 1196–1154 cm⁻¹ belong to C–O stretching of ester

group and that at 991–961 cm⁻¹ refers to C–H bending (Swain *et al*., 2010).
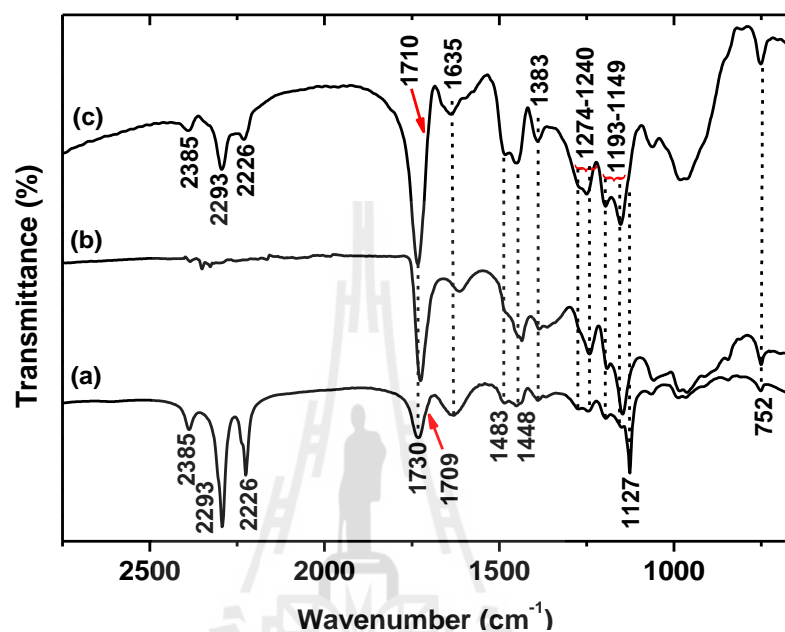
Figure 4.5 FTIR spectra of nano LiBH₄–NaAlH₄–PcB before desorption (a), after

desorption (b), and after absorption (c).

In the case of the nano LiBH₄–NaAlH₄–PcB, the sample before desorption

shows characteristic peaks of [BH₄]⁻ stretching (2385, 2293, and 2226 cm⁻¹) and

bending (1127 cm⁻¹) of LiBH₄ together with all peaks of PcB (Figure 4.5 (a)). This

suggests the existence of LiBH₄ in nano LiBH₄–NaAlH₄–PcB. Moreover, the

spectrum shows a small shoulder at 1709 cm⁻¹ refering to not only Li⁺---O=C

interaction (Lim *et al*., 2008) formed between LiBH₄ and PcB, but also probably Na⁺-

--O=C interaction between NaAlH₄ and PcB. From the previous work, vibrational

peak of B−O bonds due to B---OCH₃ interaction, hinting at LiBH₄/PcB interaction

was observed as a sharp peak at 1383 cm⁻¹ (Gosalawit–Utke *et al*., 2014). However,

for nano LiBH$_4$–NaAlH$_4$–PcB, this vibration is not obviously detected (Figure 4.4 (a)). This could be due to the fact that B---OCH$_3$ interaction (LiBH$_4$/PcB interaction) is reduced by adding small amount of NaAlH$_4$ in nano LiBH$_4$–PcB, further discussed and confirmed in section 4.5. In the case of the sample after desorption, all vibrational peaks of PcB are still observed as in case of sample before dehydrogenation. However, the vibrational peaks of B–H bond of LiBH$_4$ are not observed, demonstrating complete dehydrogenation of LiBH$_4$ (Figure 4.5 (b)). For the sample after rehydrogenation, the vibrational peaks of B–H bond from LiBH$_4$ are recovered, referring to successful reversibility of nano LiBH$_4$–NaAlH$_4$–PcB (Figure 4.5 (c)).

4.5 LiBH$_4$/PcB interaction and prevention of LiBH$_4$ oxidation in air

In order to quantitatively determine the reduction of LiBH$_4$/PcB (B---OCH$_3$) interaction, quantitative analysis by FTIR technique was carried out. Relative concentration (or amount) of the phase of interest with respect to the reference can be quantitatively determined by the ratio of their FTIR peak area (Pierce *et al*., 1990 and Xiong *et al*., 2013). In this work, phase of interest and reference are B–H (υ(B–H)) and C=O (υ(O=C)) stretching from LiBH$_4$ and PcB, respectively. The more the ratio of peak area of υ(B–H)/υ(O=C), the lower the LiBH$_4$/PcB (B---OCH$_3$) interaction.
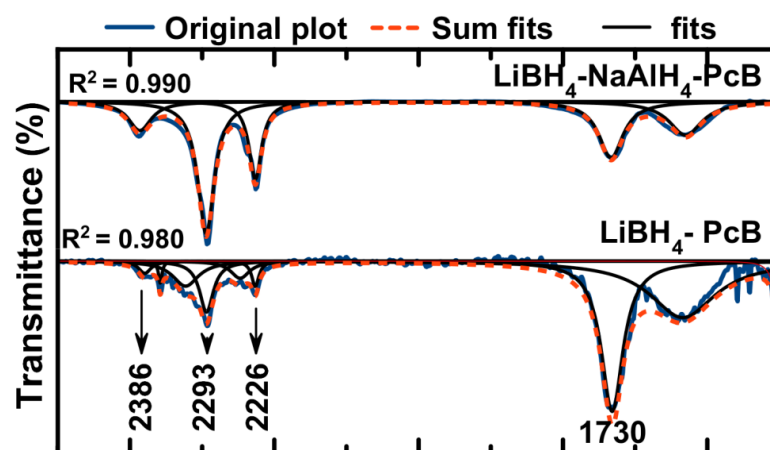
Figure 4.6 Curves fitting of FTIR spectra of nano LiBH₄–PcB and nano LiBH₄–NaAlH₄–PcB.

This results in the higher content of $[BH_4]^-$ for dehydrogenation and increase of H_2 storage capacity. The peak areas of $\upsilon(B–H)$ (in the range of 2386–2226 cm^{-1}) and $\upsilon(O=C)$ (at 1730 cm^{-1} and the shoulder due to Li$^+$/Na$^+$---O=C interaction at 1710–1708 cm^{-1}) were calculated by curve fitting method using Magic Plot program. The curve fitting results of FTIR spectra of nano LiBH₄–PcB and nano LiBH₄–NaAlH₄–PcB are shown in Figure 4.6. The peak area of both vibrations ($\upsilon(B–H)$ and $\upsilon(O=C)$) as well as the ratio of their peak area ($\upsilon(B–H)/\upsilon(O=C)$) calculated from Figure 4.6 are summarized in Table 4.2.

Table 4.2 Peak area of B–H stretching, O=C stretching, and υ(B–H)/υ(O=C) ratio of nanoconfined samples.

Nanoconfined samples	Peak area		υ(B–H)/υ(O=C) ratio
	υ(B-H) (2226-2386 cm^{-1})	υ(O=C) (1730 cm^{-1})	
LiBH$_4$–PcB	109.5	171.2	0.6
LiBH$_4$–NaAlH$_4$–PcB	48.4	17.1	2.8

From Table 4.2, the υ(B–H)/υ(O=C) ratio of nano LiBH$_4$–PcB and nano LiBH$_4$–NaAlH$_4$–PcB are 0.6 and 2.8, respectively. Because of lower υ(B–H)/υ(O=C) ratio, it is clear that the nano LiBH$_4$–PcB has higher B---OCH$_3$ interaction as compared with nano LiBH$_4$–NaAlH$_4$–PcB. Therefore, it can confirm that the interaction between LiBH$_4$ with PcB is reduced by adding small amount of NaAlH$_4$. With respect to the amount of hydrogen in the 1st cycle (Figures 4.3), the higher hydrogen content released from nano LiBH$_4$–NaAlH$_4$–PcB with respect to that of nano LiBH$_4$–PcB can be due to the reduction of B---OCH$_3$ interaction. The reduction of LiBH$_4$/PcB interaction can be due to the competitive interaction of partial [AlH$_4$]$^-$ from NaAlH$_4$ with alkoxy (–OCH$_3$ and/or –OC$_4$H$_9$) groups of PcB. The interaction between [AlH$_4$]$^-$ and alkoxy groups (–OCH$_3$ and/or –OC$_4$H$_9$) is confirmed and discussed in solid-state MAS NMR results.

Moreover, to confirm the ability to prevent hydride deterioration in air of nano LiBH$_4$–PcB and nano LiBH$_4$–NaAlH$_4$–PcB as well as the reduction of LiBH$_4$/PcB (B---OCH$_3$) interaction after adding small amount of NaAlH$_4$ into nano LiBH$_4$–PcB, X-ray photoelectron spectroscopy (XPS) was used to investigate the elemental

compositions and the local chemical environment of the target elements in the sample surface (up to 10 nm depth). From Figure 4.7 (a), Li 1s of bulk $LiBH_4$ shows a peak of Li_2O at 55 eV (Deprez et al., 2011). In the case of B 1s, formations of B_xO_y (x/y = 3) and B_2O_3 are observed at 187 and 192 eV, respectively (Alexander et al., 2000; Deprez et al., 2011). The formations of Li_2O, B_xO_y (x/y = 3), and B_2O_3 refer to oxidation of $LiBH_4$ with oxygen or humidity in air. Moreover, the signal of $LiBH_4$ in Li 1s and B 1s spectra is not detected (Figure 4.7 (a)), hinting at instability of $LiBH_4$ under ambient condition (25 °C under atmospheric pressure). For nanoconfined samples, prior to the XPS experiments the samples were left in ambient environment (25 °C under atmospheric pressure) for 3 days. From Figure 4.7 (b) and (c), Li 1s of both nanoconfined samples shows characteristic peaks of LiH and $LiBH_4$ at 54.5 and 56.2 eV, respectively (Haipinga et al., 2011; Fang, et al., 2011). The signals of $LiBH_4$ found in Li 1s spectra of both nanoconfined samples confirmed that PcB is able to prevent oxidation of $LiBH_4$ under ambient condition. For LiH formation, it suggests partial dehydrogenation of $LiBH_4$ during nanoconfinement, in agreement with the inferior hydrogen content released with respect to theoretical value during the 1st dehydrogenation (Figure 4.3). In the case of B 1s, both nanoconfined samples reveal characteristic peaks of B_xO_y (x/y = 3) and $LiBH_4$ at 187 and 188 eV, respectively (Haipinga et al., 2011; Deprez et al., 2011). The formation of B_xO_y (x/y = 3) in case of nanoconfined samples hints at $LiBH_4$/PcB interaction formed between [BH_4^-] of $LiBH_4$ with $-OCH_3$ of PcB (B---OCH_3 interaction) (Gosalawit–Utke et al., 2014).
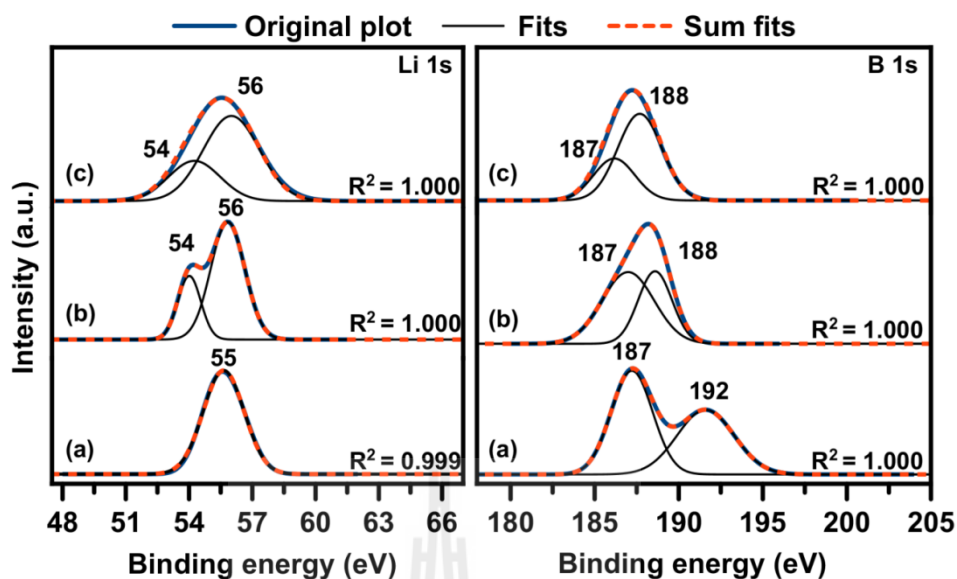
Figure 4.7 Li 1*s* and B 1*s* XPS spectra of bulk LiBH₄ (a), nano LiBH₄−PcB (b), and nano LiBH₄–NaAlH₄–PcB (c).

However, the relative amount of B_xO_y (from B---OCH₃ interaction) with respect to LiBH₄ obtained from nano LiBH₄–NaAlH₄–PcB is lower than that of nano LiBH₄– PcB (B 1*s* spectra in Figures 4.7 (b) and (c)), suggesting the reduction of LiBH₄/PcB interaction after adding small amount of NaAlH₄ into nano LiBH₄–PcB. This is in agreement with FTIR curve fitting results (Figure 4.6).

To further investigate the reason for the reduction of LiBH₄/PcB interaction, nano LiBH₄–NaAlH₄–PcB was studied by solid state ¹¹B, ²³Na, and ²⁷Al MAS NMR measurements. From Figure 4.8, ¹¹B MAS NMR spectrum of LiBH₄ shows a single peak at -41.5 ppm, corresponding to LiBH₄ reported elsewhere (Choi *et al*., 2011). In the case of nano LiBH₄–NaAlH₄–PcB, the signal of LiBH₄ at -41.5 ppm is observed together with a shoulder at -42.7 ppm, corresponding to NaBH₄ (Figure 4.8 (a)) (Garroni *et al*., 2011). This suggests partial reaction between LiBH₄ and NaAlH₄ to

produce $NaBH_4$ during sample preparation. Furthermore, the peaks of B–O bonds are found in the range of 0–20 ppm (MacKenzie and Smith, 2002), especially the main peak at 0.4 ppm corresponding to $LiBH_4$/PcB (B---OCH_3) interaction, in agreement with B $1s$ XPS results (Figure 4.7 (c)). For ^{23}Na MAS NMR, $NaAlH_4$ and the nano $LiBH_4$–$NaAlH_4$–PcB show a single peak at -9.6 ppm, corresponding to $NaAlH_4$ (Nielsen *et al*., 2014; Liang *et al*., 2011). In the case of ^{27}Al MAS NMR, $NaAlH_4$ shows a main peak at 95.6 ppm as well as a small peak at 81.3 ppm, corresponding to $NaAlH_4$ and aluminum oxide or hydroxide species (e.g., AlO_4) (Choi *et al*., 2011), respectively. For nano $LiBH_4$–$NaAlH_4$–PcB, Figure 4.8 (a) shows the signals of $NaAlH_4$ (at 95.6 ppm) together with those of aluminium alkoxide ($Al(OR)_3$) (at 50.1 and 43.6 ppm), where R could be either metyl (–CH_3) or butyl (–C_4H_9) group of PcB polymer branches (KŘÍž *et al*., 1984). A small peak at 22.2 ppm relates to β–AlH_3 (Hwang *et al*., 2007) (Figure 4.8 (a)). It can be concluded that there is not only B---OCH_3 interaction in nano $LiBH_4$–$NaAlH_4$–PcB, but also those of Al---OCH_3 and/or Al---OC_4H_9 interactions are observed. Therefore, by adding amount of $NaAlH_4$ in nano $LiBH_4$–PcB, competitive interaction of $[AlH_4^-]$/PcB is accomplished, leading to the reduction of $LiBH_4$/PcB interaction, in accordance with FTIR and XPS results. Therefore, the H_2 content released during the 1st and the 2nd desorption of nano $LiBH_4$–$NaAlH_4$–PcB is higher than that of nano $LiBH_4$–PcB (Figures 4.3 (A) and (B)).
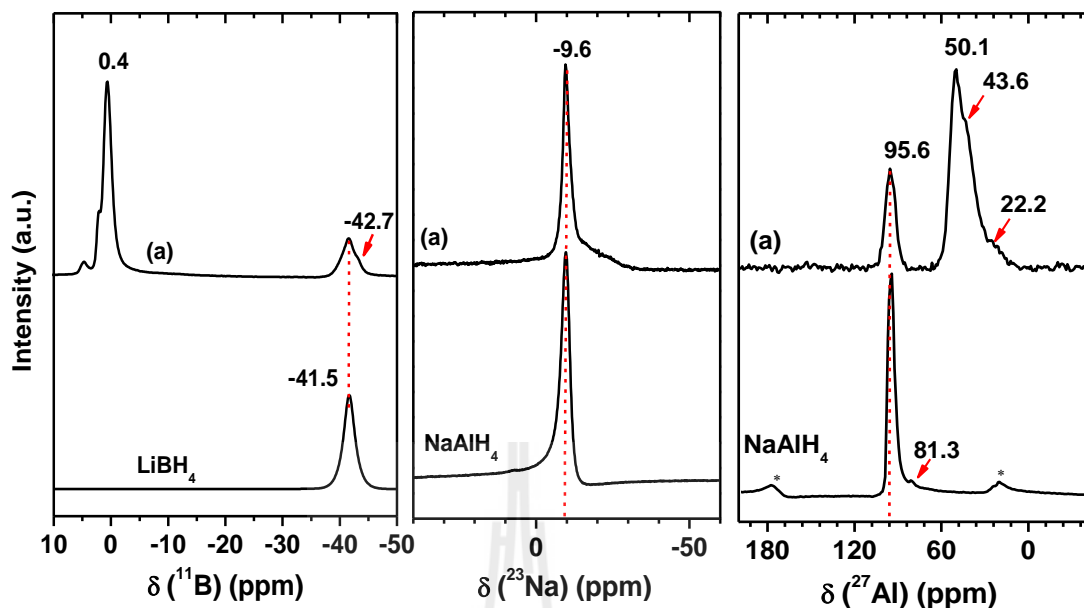
Figure 4.8 Solid state ^{11}B, ^{23}Na, and ^{27}Al MAS NMR of LiBH$_4$, NaAlH$_4$, and nano LiBH$_4$–NaAlH$_4$–PcB (a).

Furthermore, powder X–ray diffraction (XRD) of PcB and nanoconfined samples was carried out to study the effects of LiBH$_4$/PcB and NaAlH$_4$/PcB interaction on d-spacing of PcB polymer chains. From Figure 4.9 (a), pure PcB shows broad peaks at 2θ values of 13.9°, 29.7°, and 42.0° indicating amorphous nature of PcB (Gosalawit–Utke *et al*., 2014). For nanoconfined samples, splitting of XRD peak at 13.9° to higher and lower values is detected (Figures 4.9 (c) and (d)), referring to change of PcB polymer d-spacing. For nano LiBH$_4$–PcB, XRD peak at 13.9° splits into two peaks at 13.9° and 17.0° (Figure 4.9 (b)). Based on Bragg's Law, where nλ = 2dsinθ, enhancement of 2θ value means decrease of d-spacing. The peaks at 13.9° is a character of PcB polymer and at 17.0° should be due to the LiBH$_4$/PcB interaction (B---OCH$_3$ and Li$^+$---O=C). Because the LiBH$_4$/PcB interaction probably draws the PcB polymer chains to be closed to each other, d-spacing of PcB polymer decreases. In the case of nano LiBH$_4$–NaAlH$_4$–PcB, the peak shifts toward the higher and lower 2θ

values of 17.0° and 12.4°, respectively (Figure 4.9 (c)). For the peak at 17.0°, it refers to LiBH₄/PcB interaction as explained in the XRD pattern of nano LiBH₄/PcB (Figure 4.9 (b)). The peak at 12.4° leads to higher d-spacing of PcB polymer chains, probably relating to NaAlH₄/PcB interaction. Due to the higher dissociation enthalpy of B-O bond (ΔH = 808 kJ/mol) as compared with that of Al-O bond (ΔH = 511 kJ/mol) (Luo, 2007), the interaction of LiBH₄/PcB is stronger than that of NaAlH₄/PcB. Therefore, the d-spacing of B-O bond is smaller than that of Al-O bond. Moreover, the atomic size of Li, smaller than that of Na, could probably corresponds to the lower d-spacing of PcB in nano LiBH₄–PcB with respect to that of nano LiBH₄–NaAlH₄–PcB. From these results, it can conclude that there is not only LiBH₄/PcB interaction observed, but also that of NaAlH₄/PcB interaction is observed.
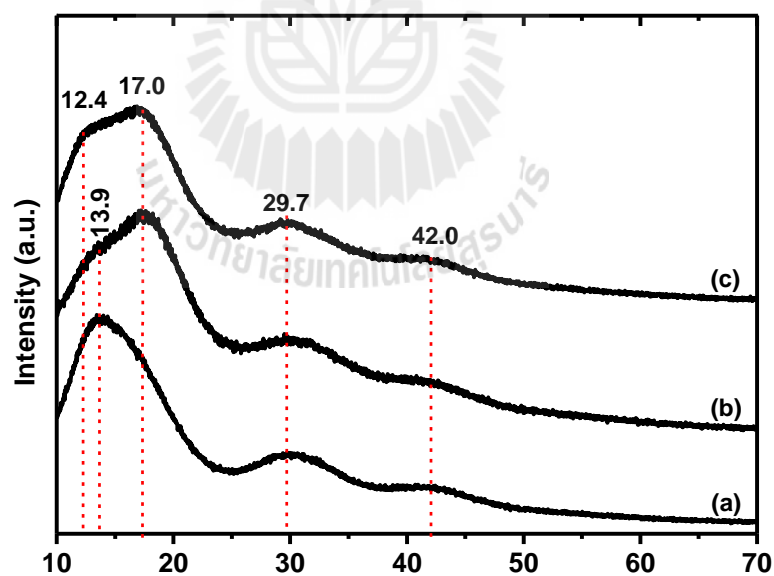

Figure 4.9 XRD patterns of PcB (a), nano LiBH₄–PcB (b) and nano LiBH₄–NaAlH₄–PcB (c).

4.6 Thermal stability

To study the effects of $NaAlH_4$ on thermal stability of nano $LiBH_4$–PcB, gas analysis was performed in the temperature range of 30-300 °C (dT/dt = 5 °C/min) under dynamic vacuum. From gas analysis results, the main gas released from nano $LiBH_4$–PcB and nano $LiBH_4$–$NaAlH_4$–PcB is hydrogen (H_2) together with gases due to thermal degradation of PcB; that is, methyl radical (•CH_3), carbon monoxide (CO), metoxy radical (•OCH_3), carbon dioxide (CO_2), and butoxy radical (•OC_4H_9) (Figures 4.10 (A) and (C)) (Kashiwagi and Inabi, 1989; Rajkumar et al., 2010; Chang et al., 2001). Therefore, this can be concluded that not only H_2 releases from nanoconfined samples, but also other gases due to thermal degradation of PcB polymer. Figures 4.7 (B) and (D) are the plots between peak area of each gas signal versus temperature from gas analyses in Figures 4.7 (A) and (C), respectively. Nano $LiBH_4$–PcB shows onset temperature (T_i) of H_2 release at ~80 °C. The main hydrogen desorption temperature (T_p) is at 105 °C and the H_2 signal finishes (T_f) at 135 °C (Figures 4.7 (B)). In the case of nano $LiBH_4$−$NaAlH_4$−PcB, it starts (T_i) and finishes (T_f) at 95 and 165 °C, respectively, while the main H_2 desorption temperature (T_p) is at 125 °C (Figure 4.10 (D)). For thermal degradation of PcB from nano $LiBH_4$–PcB, combination of gases (•CH_3, CO, •OCH_3, CO_2, and •OC_4H_9) are observed during dehydrogenation range (80-135 °C), and especially CO_2, •CH_3 and •OC_4H_9 are firstly detected approximately at onset dehydrogenation temperature (T_i) (~ 80 °C) (Figure 4.7 (B)). Moreover, significant amount of •CH_3 (59 % with respect to the highest content of hydrogen released) is detected at ~145 °C. Considerable amount of gases obtained from thermal degradation of PcB during dehydrogenation of nano $LiBH_4$− PcB hits at thermal instability of PcB host. For nano $LiBH_4$−$NaAlH_4$−PcB, the peak

area of gases release due to thermal degradation of PcB is reduced, suggesting that thermal stability of PcB is improved by adding small amount of NaAlH4.

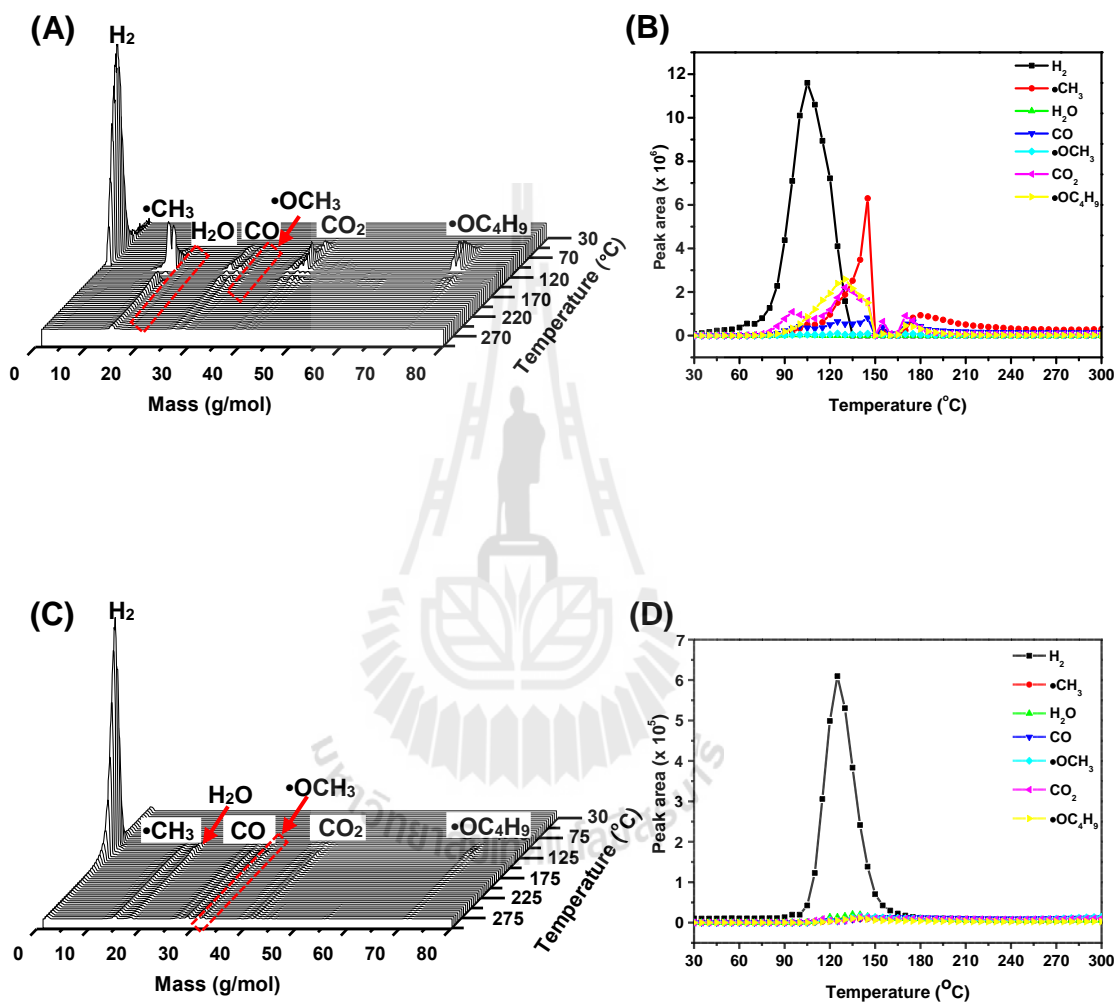**Figure 4.10** Gas analysis during dehydrogenation of nano LiBH4–PcB (A), and nano LiBH4−NaAlH4−PcB (C), and peak area of gas desorption from thermal degradation of PcB with respect to H2 at 120 °C of nano LiBH4–PcB (B), and nano LiBH4−NaAlH4−PcB (D).

Moreover, the relative amounts of gases desorbed with respect to hydrogen content at dehydrogenation temperature (120 °C) of nanoconfined samples were studied.

Table 4.3 Amount of gas desorption from thermal degradation of PcB with respect to H_2 at 120 °C.

Nanoconfined samples	Desorption temperature (°C)			Amount of gases desorbed with respect to that of H_2 at 120 °C (%)						
	T_i	T_p	T_f	•CH_3	H_2O	CO	•OCH_3	CO_2	•OC_4H_9	Total
LiBH$_4$–PcB	80	105	135	13.4	0	6.9	0.8	16.3	26.9	64.3
LiBH$_4$–NaAlH$_4$–PcB	95	125	165	1.0	2.8	1.1	1.3	1.1	0.6	7.9

T_i = Onset temperature, T_p = peak temperature and T_f = end temperature

From Table 4.3, the relative amounts of •CH_3, CO, •OCH_3, CO_2, and •OC_4H_9 with respect to H_2 content of nano LiBH$_4$–PcB and nano LiBH$_4$–NaAlH$_4$–PcB are totally 64.3 and 7.3 %, respectively. This hits at significant reduction of gases desorbed due to thermal degradation of PcB by adding small amount of NaAlH$_4$ in nano LiBH$_4$–PcB. This refers to significant improvement in thermal stability of PcB. The improvement in thermal stability of PcB is probably due to the interaction of PcB with metal hydrides; i.e., LiBH$_4$ and NaAlH$_4$, as explained in section 4.1.5, leading to the restriction of PcB polymer chain motion. Moreover, thermal stability of polymer could be improved by compositing with metal or metal ion. Thus, in the case of nano LiBH$_4$–NaAlH$_4$–PcB, not only Li$^+$---O=C interaction is observed, but also that of Na$^+$ from NaAlH$_4$ (Na$^+$---O=C interaction) is probably achieved. As reported by Lekesiz *et al*. (2014), thermal stability of polystyrene–block–poly (2–vinylpyridine) (PS–b–

P2VP) polymer was improved by compositing with metal or metals ion (Co, Cr, and Au^{3+}). They found that the more the interaction between polymer and metal (or metal ion), the higher the thermal stability.

CHAPTER V

CONCLUSION

In this thesis, nano $LiBH_4$–$NaAlH_4$–PcB was proposed for reversible hydrogen storage. The reduction of $LiBH_4$/PcB interaction (B---OCH_3) and improvement of thermal stability of PcB polymer were developed by adding small amount of $NaAlH_4$ (1.2 wt.%) . The $LiBH_4$/PcB interaction of the nanoconfined samples was analyzed quantitatively by using FTIR technique, the ratio of the peak area between B–H stretching (from $LiBH_4$) and C=O stretching (from PcB) (ν(B–H)/ν(C=O)), corresponding to the relative amount of $[BH_4]^-$ with respect to PcB, was determined. The more the (ν(B–H)/ν(C=O)) ratio, the higher the free $[BH_4]^-$ content and the lower the $LiBH_4$/PcB interaction. The (ν(B–H)/ν(C=O)) ratio of the nano $LiBH_4$–PcB and nano $LiBH_4$–$NaAlH_4$–PcB were 0.6 and 2.8, respectively. Therefore, it could be confirmed that $LiBH_4$/PcB interaction was decreased by adding small amount of $NaAlH_4$. From the B $1s$ XPS result, the relative amount of B_xO_y (from B---OCH_3 interaction) with respect to $LiBH_4$ of nano $LiBH_4$–$NaAlH_4$–PcB was lower than that of nano $LiBH_4$–PcB. In addition, the solid state MAS NMR and XRD results of nano $LiBH_4$–$NaAlH_4$–PcB confirmed that the $LiBH_4$/PcB interaction was decreased due to the competitive reaction of $[AlH_4]^-$ (of $NaAlH_4$) with –OCH_3 and/or –OC_4H_9 (of PcB). These result in increase of H_2 content desorbed during the 1st and 2nd dehydrogenations of nano $LiBH_4$–$NaAlH_4$–PcB as compared with nano $LiBH_4$–PcB. Moreover, the total amount of gases desorbed due to thermal degradation of PcB with

respect to H_2 content at 120 °C from nano LiBH$_4$–PcB and nano LiBH$_4$–NaAlH$_4$–PcB were 64.3 and 7.9 %, respectively. This could be due to not only the interaction of PcB at methoxyl and/or buthoxyl groups with metal hydrides (LiBH$_4$ and NaAlH$_4$), but also that of carbonyl group (from PcB) with metal ions (Li$^+$ and Na$^+$). In conclusion, the reduction of LiBH$_4$/PcB interaction and the improvement of thermal stability of nano LiBH$_4$–PcB were obtained by doping with small amount of NaAlH$_4$.

REFERENCES
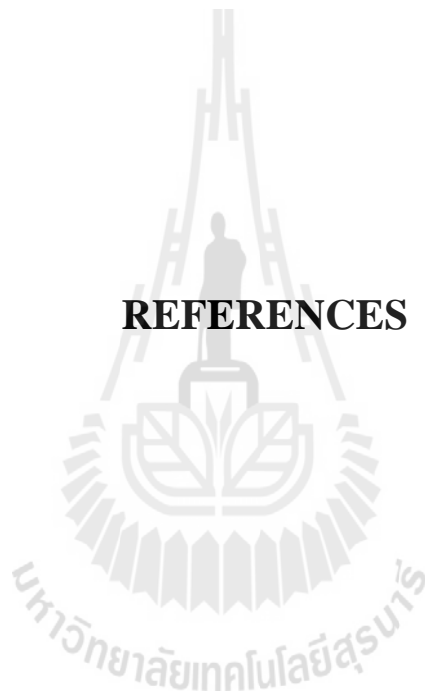
REFERENCES

Ahmad, A., Rahman, A., Su'ait, S., and Hamzah, H. (2011). Study of MG49-PMMA Based Solid Polymer Electrolyte. **TOMSJ.** 5: 170-177.

Alexander, V. (2000). NIST X-ray Photoelectron Spectroscopy Database**.** [On-line]. Available: http://srdata.nist.gov/xps/selEnergyType.aspx.

Aoki M., Miwa K., Noritake T., Kitahara G., Nakamori Y., Orimo S., and Towata S. (2005). Destabilization of $LiBH_4$ by mixing with $LiNH_2$. **Appl. Phys. A.** 80: 1409-1412.

Bal, S., and Sama, S. (2007). Carbon nanotube reinforced polymer composite-A state of the art. **B. Mater. Sci.** 30: 86-379.

Basic research needs for the hydrogen economy, Second Printing. (2004). **Basic Research Challenges for Hydrogen Storage.** (pp. 31-51). Washington, DC: U.S. Department of Energy.

Blanchard D., Shi Q., Boothroyd C. B., and Vegge T. (2009). Reversibility of Al/Ti Modified $LiBH_4$. **J. Phys. Chem. C.** 113: 14059-14066.

Bogdanovic, B., Hartwig, T., and Spliethoff, B. (1993). The development, testing and optimization of energy storage materials based on the MgH_2Mg system. **Int. J. Hydrogen Energy.** 18: 575-589.

Bogdanovic, B., and Schwickardi, M. (1997). Ti-doped alkali metal aluminium hydrides as potential novel reversible hydrogen storage materials. **J. Alloys. Compd.** 1-9: 253-254.

Bogdanovic, B., Brand, A., Schwickardi, M., and Tolle, J. (2000). Metal-doped sodium aluminium hydrides as potential new hydrogen storage materials. **J. Alloys. Compd.** 302: 36-58.

Bogdanovic, B., Felderhoff, M., Pommerin, A., Schüth, F., and Spielkamp, N. (2006). Advanced hydrogen storage materials based on Sc-, Ce-, and Pr-doped $NaAlH_4$. **Adv. Mater.** 18: 1198-1201.

Carrette, L., Friedrich, K. A., and Stimming, U. (2001). **Fuel Cells-fundamental and application.** (pp. 1-2). Weinheim: WILEY-VCH Verlag GmbH.

Choi, J., Lu, J., Sohn, Y., Fang, Z., Kim, C., and Bowman, C. (2011). Reaction Mechanism in the Li_3AlH_6/$LiBH_4$ and Al/$LiBH_4$ System for Reversible Hydrogen Storage. Part 2: Solid-state NMR Studies. **J. Phys. Chem. C.** 115: 6048-6056.

Dell, R. M., and Rand, D. A. J. (2001). Energy storage-a key technology for global energy sustainability. **J. Power Sources.** 100: 2-17.

Deprez, E., Munoz-Marquez, A., Jimenez de Haro, C., Palomares, J., Soria, F., Dornheim, M., Bormann, R., and Fernandez, A. (2011). Combined x-ray photoelectron spectroscopy and scanning electron microscope studied of the $LiBH_4$−MgH_2 reactive hydride composite with and without a Ti−based additive. **J. Appl. Phys.** 109: 014913-10.

Dorthe, B., Ravnsbaek, Torben, R., and Jensen. (2010). Tuning hydrogen storage properties and reactivity: Investigation of $LiBH_4$–$NaAlH_4$ system. **J. Phys. Chem. Solids.** 71: 1144-1149.

Dresselhaus, M. S., and Thomas, I. L. (2001). Alternative energy technologies. **Nature.** 414: 332-337.

Energy Resources. (2014). [On-line]. Available: http://nurer2014.org/.

Environmental and Energy Study Institute. (2014). Environmental and Energy Study Institute. (2014). [On-line]. Available: http://www.eesi.org/.

Fang, Z., Kang, D., Yang, X., Walker, S., and Wang, P. (2011). Combined effects of functional cation and anion on the reversible dehydrogenation of LiBH4. **J. Phys. Chem. C.** 115: 11839-11845.

Fichtner, M. (2005). Nanotechnological aspects in materials for hydrogen storage. **Adv. Eng. Mater.** 7: 443-455.

Fu, J., Ramirez-Cuesta, J., and Tsang, C. (2006). Molecular aluminum hydrides NaAlH$_4$. **J. Phys. Chem. B.** 11: 711-715.

Fuel Cells Fuel Alternative Energy Options. (2013). [On-line]. Available: http://energydesignresources.com/resources/e-news/e-news-90-fuel-cells.aspx.

Garroni, S., Milanese, C., Pottmaie,r D., Mulas, G., Nolis, P., and Girella, A. (2011). Experimental Evidence of Na$_2$[B$_{12}$H$_{12}$] and Na Formation in the Desorption Pathway of the 2NaBH$_4$+MgH$_2$ System. **J. Phys. Chem. C.** 115: 16664-71.

Gosalawit–Utke, R., Meethom, S., Pistidda, C., Milanese, C., Laipple, D., Saisopa, T., Marini, A., Klassen, T., and Dornheim, M. (2014). Destabilization of LiBH$_4$ by nanoconfinement in PMMA-co-BM polymer matrix for reversible hydrogen storage. **Int. J. Hydrogen Energy.** 39: 5019-29.

Grochala, W., and Edwards, P. (2004). Thermal Decomposition of the Non-Interstitial Hydrides for the Storage and Production of Hydrogen. **Chem. Rev.** 104: 1283.

Gross, F., Vajo, J., Van Atta, L., and Olson, L. (2008). Thermal Decomposition of the kinetics in nanoporous carbon scaffold. **J. Phys. Chem. C.** 112: 5651-5657.

Huang, J., Yan, Y., Ouyang., L, Wang, H., Liu, J., and Zhua, M. (2014). Increased air

stability and decreased dehydrogenation temperature of LiBH$_4$ via modification within poly(methylmethacrylate). **R. Soc. Chem.** 43: 410-413.

Haipinga, W., Tiechengb, L., Xuemina, W., Fangfanga, G., Linhonga, C., Honglianga, Z., Chunhonga, L., Xiaohanc, Y., Xind, J., and Weidonga, W. (2011). Corrosion characteristics of LiBH$_4$ film exposed to a CO$_2$/H$_2$O/O$_2$/N$_2$ mixture. **Corros. Sci.** 53: 1115-1119.

Hwang, J., Bowman, C., Graetz, J., Reilly, J., Langley, W., and Jensen, M. (2007). NMR studies of the aluminium hydride phases and their stabilities. **J. Alloys. Compd.** 5-290: 446-447.

Hydrogen powered cars. (2013). [On-line]. Available: http://www.engineering.com/DesignerEdge/DesignerEdgeArticles/ArticleID/59 74/Hydrogen-Powered-Cars--Coming-to-a-highway-near-you.aspx.

Jain, P., Lal, C., and Jain, A. (2010). Hydrogen storage in Mg: A most promising material. **Int. J. Hydrogen Energy.** 35: 5133-5144.

Jeon, J., Moon, R., Ruminski, M., Jiang, B., Kisielowski, C., Bardhan, R., and Urban, J. J. (2011). Air-stable magnesium nanocomposites provide rapid and high-capacity hydrogen storage without using heavy-metal catalysts. **Nat. Mater.** 10: 286-290.

Kashiwaki, T., Inaba, A., Brown, J., Hatada, K., Kitayama, T., and Masuda, E. (1986). Effects of weak linkages on the thermal and oxidative degradation of poly(methyl methacrylates). **J. Am. Chem. Soc.** 19: 2160-2168.

Kashiwagi, T., Inaba, A., and Hamins, A. (1989). Behavior of primary radicals during thermal degradation of poly (methyl methacrylate). **Polym. Degrad. Stab.** 26: 84-161.

KŘÍž, O., ČÁSENSKÝ, B., LYčKA, A., FUSEK, J., and HEŘMÁNEK, S. (1984). ^{27}Al NMR Behavior of Aluminum Alkoxides. **J. Magn. Reson**. 60: 375-381.

Lekesiz, O., Kaleli, K., Uyar, T., Kayran, C., and Hacaloglu, J. (2014). Preparation and characterization of polystyrene-b-poly-(2-vinylpyridine) coordinated to metal or metal ion nanoparticles. **J. Anal. Appl. Pyrol.** 106: 81-85.

Liang, C., Liu, F., Jiang, Y., Wei, Z., Gao, M., Pan, H., and Wang, Q. (2011). Local defects enhanced dehydrogenation kinetics of the $NaBH_4$-added Li–Mg–N–H system. **J. Phys. Chem.** 13: 314-321.

Liang, C., Liu, F., Fu, L., Ding, F., Gao, X., and Pan, G. (2011). Li–Mg–N–H-based combination systems for hydrogen storage. **J. Alloys. Compd.** 509: 7844-7853.

Lim, S., Noda, I., and Im, S. (2008). Effects of metal ion-carbonyl interaction on miscibility and crystallization kinetic of poly(3-hydroxybutyrate-co-3-hydroxyhexanoate)/lightly ionized PBS. **Eur. Polym. J.** 44: 1428-1440.

Liu X., Peaslee D., Jost C. Z., and Majzoub E. H. (2010). Controlling the decomposition Pathway of $LiBH_4$ via confinement in highly ordered nanoporous carbon. **J. Phys. Chem. C.** 114: 14036-14041.

Luo, R. (2007). **Comprehensive Handbook of Chemical Bond Energies.** (pp. 9-79). United States of America: CRC Press.

Mackenzie, D., and Smith, E. (2002). **Multinuclear Solid-State NMR of Inorganic Materials.** (pp. 330). United Kingdom: Pergamon Materials Series.

Majzoub, H., and Gross, J. (2003). The reversible hydrides solution for hydrogen storage. **J. Alloys. Compd.** 356-357: 363-367.

Mark, E. (1999). **Polymer Data Handbook.** (pp. 9-79). New York, NY: Oxford University Press.

Michael, B. (2014). **Solar Electricity Handbook: A Guide to Solar Energy**. (pp. 5-9). USA: Springer Science and Business Media.

Mori, D. and Hirose, K. (2009). Recent challenges of hydrogen storage technologies for fuel cell vehicles. **Int. J. Hydrogen Energy.** 34(10): 4569-4574.

Nakamori, Y., Miwa, K., Ninomiya, A. Li, H., Ohba, N., Towata, S. (2006). Correlation between thermodynamical stabilities of metal borohydrides and cation electronegativites: First-principles calculations and experiments. **Phys. Rev. B.** 74: 045126-045134.

Natural Gas Vehicles for America. (2011). Technology. [On-line]. Available: http://www.ngvc.org/tech_data/index.html.

Nielsen, K., Javadian, P., Polanski, M., Besenbacher, F., Bystrzycki, J., Skibsted, J., and Jensen, R. (2014). Nanoconfined NaAlH$_4$: prolific effects from increased surface area and pore volume. **J. R. Soc. Chem.** 6: 599-607.

Ozolins, V., Majzoub, H., and Udovic, J. (2004). Electronic structure and rietveld refinement parameters of Ti-doped sodium alanates. **J. Alloys. Compd.** 375: 1-10.

Pierce, A., Jackson, S., Van, W., Griffiths, R., and Gao, H. (1990). Combined deconvolution and curve fitting for quantitative analysis of unresolved spectral bands. **Anal. Chem.** 62: 477-84.

Problems and Dangers of Nuclear Energy. (2014). [On-line]. Available: http://www.buzzle.com/articles/nuclear-energy-problems-and-dangers.html.

Prototype tank for NaAlH$_4$ based solid state hydrogen storage. (2010). [On-line]. Available: http://www.flyhy.eu/structure.html.

Rafi-ud-din, Xuanhui, Q., Ping, L., Zhang, L., Qi, W., Iqbal, Z., and Rafique, Y. (2012). Implementing a hydrogen economy. **Mater. Today 6.** 9: 18-23. Superior Catalytic Effrcts of Nb_2O_5, TiO_2, and Cr_2O_3 Nanoparticles in Improving the Hydrogen Sorption Properties of $NaAlH_4$. **J. Phys. Chem. C.** 116: 11924-38.

Ritter, A., Ebner, D., Wang, J., and Zidan, R. (2003). Implementing a hydrogen economy. **Mater. Today 6.** 9: 18-23.

Rongeata, C., Annac, D., Hagemannc, H., Borgschulteb, A., Züttelb, A., Schultza, L., and Gutfleischa, O. (2010). Effect of additives on the synthesis and reversibility of $Ca(BH_4)_2$. **J. Alloys. Compd.** 493: 281-287.

Sandi, G. (2004). "Hydrogen storage and its limitations," The Electrochem. **Soc. Interface.** 13: 40-44.

Schlapbach, S., and Züttel, A. (2001). **Hydrogen storage materials for mobile.** (pp. 5) **Berlin**: Springer, Heidelberg: 113-213.

Seidl, J., Malinský, J., Dušek, K., and Heitz, W. (1967). In Fortschritte der Hochpolymeren-Forschung. **Nature.** 414: 353-358.

Schwartz, M. (1978). Schlapbach, S., and Züttel, A. (2001). The Benzophenone/Ketyl Tetrahydrofuran (THF). **Still. Chem. Eng. News.** 24: 88.

Shi, Q., Yu, X., Feidenhans'l, R., and Vegge, T. (2008). Destabilized $LiBH_4$-$NaAlH_4$ Mixtures Doped with Titanium Based Catalysts. **J. Phys. Chem. C.** 112: 18244-18248.

Stambouli, B., and Traversa, E. (2002). Fuel cell, an alternative standard sources of energy. **Renew. Sust. Energ. Rev.** 6: 297-306.

Stampfer, J., Holley, C., and Suttle, J. (1960). The Magnesium-Hydrogen System. **J. Am. Chem. Soc.** 82: 3504-3508.

Sun, D., Kiyobayashi, T., Takeshita, T., Kuriyama, N., and Jensen, M. (2002). X-ray diffraction studies of titanium and zirconium doped $NaAlH_4$: euclidation of doping induced structural changes and their relationship to enhanced hydrogen storage properties. **J. Alloys. Compd.** 337: 8-11.

Sun, D., Srinivasan, S., Kiyobayashi, T., Kuriyama, N., and Jensen, M. (2003). Rehydrogenation of dehydrogenated $NaAlH_4$ at low temperature and pressure. **J. Phys. Chem. B.** 17: 1176-1179.

Singh, R., Kulkarni, S., and Naik, N. (2013). Effect of nano sized transition metal salts and metals on thermal decomposition behavior of polyvinyl alcohol. **Adv. Mat. Lett.** 4: 82-88.

Swain, K., and Jena, I. (2010). Polymer/carbon nanotube nanocomposites: A novel material. **Asian. J. Chem.** 22: 1-15.

Tang, E., Cheng, G., and Ma, X. (2006). Preparation of nano-ZnO/PMMA composite particles via grafting of the copolymer onto the surface of zinc oxide nanoparticles. **Powder. Technol.** 161: 209-214.

Thakur, K., and Shukla, N. (2009). Role of salt concentration on conductivity optimization and structural phase separation in a solid polymer electrolyte based on PMMA-$LiClO_4$. **Ionics.** 15: 357-367.

Tomar, K., Mahendia, S., and Kumar, S. (2011). Structural characterization of PMMA blended with chemically synthesized PAni. **Adv. Appl. Sci. Res.** 2: 327-333.

Tomioka, J. I., Kiguchi, K., Tamura, Y., Mitsuishi, H. (2011). Influence of temperature on the fatigue strength of compressed-hydrogentanks for vehicles. **Int. J. Hydrogen Energy.** 36: 2513-2519.

U.S. DOE, Office of EERE, Alternative & Advanced Vehicles. (2010). **What is a fuel cell vehicle.** [On-line]. Available: http://www.afdc.energy.gov/afdc/vehicle /fuel_cell_what_is.html.

U.S. DOE, Office of EERE, fueleconomy.gov. (2011). **Fuel Cell Vehicles.** [On-line]. Available: http://www.fueleconomy.gov/feg/fuelcell.shtml.

Vajo, J., Mertens, F., Ahn, C., Bowman, R., and Fultz, B. (2004). Altering Hydrogen Storage Properties by Hydride. **J. Phys. Chem. B.** 108: 13977-13983.

Vajo, J., Skeith, S., and Mertens, F. (2005). Reversible storage of hydrogen in destabilized $LiBH_4$. **J. Phys. Chem. B.** 109: 3719-3722.

Vajo, J., and Olson, G. (2007). Hydrogen storage in destabilized chemical, systems **Scripta. Mater.** 56: 829.

Vajo, J., Li, W., and Liu, P. (2010). Thermodynamic and kinetic destabilization in $LiBH_4/Mg_2NiH_4$: promise for borohydride-based hydrogen storage. **Chem. Comm.** 46: 6687-6689.

Varin, A., Czujko, T., and Wronski, S. (2009). **Nanomaterials for Solid State Hydrogen Storage.** (pp. 3-4). USA: Springer Science and Business Media.

Viratyaporn, W., and Lehman, L. (2011). Effect of nanoparticles on the thermal stability of PMMA nanocomposites prepared by in situ bulk polymerization. **J. Therm. Anal. Calorim.** 103: 267-73.

Wang, Q., Chen, U., Tao, D., and Wu, L. (2008). Review on hydrogen storage properties and reaction mechanism of metal-NH systems. **Rare. Met. Mater. Eng.** 37: 382-385.

Xia L., Guo H., Wu, Z., and Yu, B. (2009). Enhanced hydrogen storage performance of $LiBH_4$–Ni composite. **J. Alloys. Compd.** 479: 545-548.

Xiong, Y., Chen, G., Guo, S., and Li, G. (2013). Lifetime prediction on NBR composite sheet in aviation kerosene by using nonlinear curve fitting of ATR–FTIR spectra. **J. Ind. Eng. Chem.** 19: 1606-1611.

Yang, J., Sudik, A., and Wolverton, C. (2007). Destabilizing $LiBH_4$ with a Metal (M = Mg, Al, Ti, V, Cr, or Sc) or Metal Hydride ($MH_2 = MgH_2$, TiH_2, or CaH_2). **J. Phys. Chem. C.** 111: 19134-19140.

Yang, Y., Liu, Y., Wu, H., Zhou, W., Gao, M., and Pan, H. (2014). An ammoniastabilized mixed-cation borohydride: synthesis, structure and thermal decomposition behavior. **Phys. Chem. Chem. Phys.** 16: 135-143.

Yu X., Xia G., Guo. Z., and Liu, K. (2009). Dehydrogenation/rehydrogenation mechanism in aluminum destabilized lithium borohydride. **J. Mater. Res.** 24: 2720-2727.

Zhang, Y., Zhang, W. S., Wang, A. Q., Suna, L. X., Fana, Me. Q., Chua, H. L. et al. (2007). $LiBH_4$ nanoparticles supported by disordered mesoporous carbon: Hydrogen storage performances and destabilization mechanisms. **Int. J. Hydrogen Energy.** 32: 3976-3980.

Zhang. Y., Tian. Q., Chu. H., Zhang. J., Sun. L., Sun. J., and Wen. Z. (2009). Hydrogen de/resorption properties of $LiBH_4$-MgH_2-Al. **J. Phys. Chem. C.** 113: 21964-21969.

Züttel, A. (2003). Materials for hydrogen storage. **Mater. Today 6.** 9: 24-33.

Züttel, A. (2004). Hydrogen storage methods. **Naturwissenschaften.** 91: 157-172.

Züttel, A., Rentsch, S., Fisher, P., Wenger, P., Sudan, P., Mauron, Ph., a
    Emmenegger, Ch. (2003). Hydrogen storage properties of LiBH4. **J. Alloys.**
    Compd. 356-357: 515-520.

APPENDIX

APPENDIX

CALCULATION OF HYDROGEN CAPACITY

A.1 Calculation of theoretical hydrogen storage capacity

➢ **Nano LiBH$_4$–PcB**

Amount of PcB (5.0656g) and LiBH$_4$ (0.66 g), wt.% of LiBH$_4$ in PcB is calculated by:

$$\text{Wt.\% of LiBH}_4 = 0.66 \text{ g} / (5.0656 \text{ g} + 0.66 \text{ g}) \times 100$$

$$= 11.53 \text{ wt.\%}$$

From 13.8 wt.% of hydrogen released by pure LiBH$_4$, the theoretical of hydrogen capacity of nanoconfined LiBH$_4$–PcB is calculated by:

$$\text{Wt.\% of hydrogen} = (13.8 \text{ wt.\%} \times 11.53 \text{ wt.\%}) / 100$$

$$= 1.60 \text{ wt.\% H}_2$$

➢ **Nano LiBH$_4$–NaAlH$_4$–PcB**

Amount of PcB (0.5144), LiBH$_4$ (0.066) and NaAlH$_4$ (0.007), wt.% of LiBH$_4$ and NaAlH$_4$ in PcB is calculated by:

$$\text{Wt.\% of composite} = 0.5144 \text{ g} + 0.066 \text{ g} + 0.007 \text{ g}$$

$$= 0.5874 \text{ g}$$

$$\text{Wt.\% of LiBH}_4 = (0.066 \text{ g} / 0.5874 \text{ g}) \times 100$$

$$= 11.23 \text{ wt.\%}$$

From 13.8 wt.% of hydrogen released by pure $LiBH_4$, the theoretical of hydrogen capacity of $LiBH_4$ in nanoconfined $LiBH_4$–$NaAlH_4$–PcB is calculated by:

$$Wt.\% \text{ of hydrogen} = (13.8 \text{ wt.\%} \times 11.23 \text{ wt.\%}) / 100$$

$$= 1.55 \text{ wt.\% } H_2$$

A.2 Calculation of hydrogen desorption capacity

1. Nano $LiBH_4$–PcB

- 1st dehydrogenation

    $T = 120 \text{ °C}$

    $P_1 = -1.33 \text{ atm}$

    $P_2 = -0.60 \text{ atm}$

    $V = 0.024 \text{ L}$

    $R = 0.0821 \text{ L atm K}^{-1} \text{ mol}^{-1}$

    $$(\Delta P)V = nRT$$

$n = [(-0.60 \text{ atm})-(-1.33 \text{ atm})] \times 0.024 \text{ L}/ [(0.0821 \text{ L atm K}^{-1} \text{ mol}^{-1}) \times 393 \text{ K}]$

   $= 5.43 \times 10^{-4} \text{ mol}$

$H_2 \text{ desorbed (wt.\%)} = [(n \times 2.0158)/\text{sample weight}] \times 100$

   $= [(5.43 \times 10^{-4} \text{ mol x } 2.0158 \text{ g/mol})/ 0.1402 \text{ g}] \times 100$

   $= 0.78 \text{ wt.\% } H_2$

- 2nd dehydrogenation

    $P_1 = -1.33 \text{ atm}$

    $P_2 = -1.04 \text{ atm}$

$n = [(-1.04 \text{ atm})-(-1.33 \text{ atm})] \times 0.024 \text{ L}/ [(0.0821 \text{ L atm K}^{-1} \text{ mol}^{-1}) \times 393 \text{ K}]$

   $= 2.16 \times 10^{-4} \text{ mol}$

H_2 desorbed (wt.%) = [(2.16 × 10⁻⁴ mol × 2.0158 g/mol)/ 0.1402 g] × 100

  = 0.32 wt.% H_2

2. Nano LiBH₄–NaAlH₄–PcB

- 1ˢᵗ dehydrogenation

  T = 120 °C

  P_1 = -1.29 atm

  P_2 = -0.60 atm

  V = 0.023 L

  R = 0.0821 L atm K⁻¹ mol⁻¹

  $(\Delta P)V = nRT$

  n = [(-0.60 atm)-(-1.30 atm)] × 0.023 L/ [(0.0821 L atm K⁻¹ mol⁻¹) × 393 K]

  = 4.99 × 10⁻⁴ mol

H_2 desorbed (wt.%) = [(n × 2.0158)/sample weight] × 100

  = [(5.43 × 10⁻⁴ mol x 2.0158 g/mol)/ 0.0861 g] × 100

  = 1.29 wt.% H_2

- 2ⁿᵈ dehydrogenation

  P_1 = -1.33 atm

  P_2 = -1.04 atm

  n = [(-0.90 atm)-(-1.30 atm)] ×0.023 L/ [(0.0821 L atm K⁻¹ mol⁻¹) × 393 K]

  = 2.85 × 10⁻⁴ mol

H_2 desorbed (wt.%) = [(2.85 × 10⁻⁴ mol × 2.0158 g/mol)/ 0.0861 g] × 100

  = 0.67 wt.% H_2

CURRICULUM VITAE

Name   Miss Nuntida Wiset

Date of Birth   18 July 1988

Address   22 Moo 4, Kantharalak, Srisaket, 33110, Thailand

Education

2007-2010   B.Sc. (Chemistry), Khon Kaen University, Thailand

2010-present   M.Sc. Program in Chemistry, Suranaree University of

                     Technology, Thailand